1–3-Type Composites Based on Ferroelectrics: Electromechanical Coupling, Figures of Merit and Piezotechnical Energy-Harvesting Applications

Christopher R. Bowen,*[a] Vitaly Yu. Topolov,[b] Yan Zhang,[c] and Alexander A. Panich[d]

Abstract: The physical and microgeometric factors that able to improve the piezoelectric performance, anisotropy and energy-harvesting characteristics of modern 1–3-type composites based on ferroelectrics are discussed. The composite connectivity patterns of particular interest for this study include 1–3–0, 1–0–3 and 1–2–2. The active components of the studied composites are chosen from either conventional perovskite-type ferroelectric ceramics, lead free materials or domain-engineered single crystals which exhibit particularly intriguing electromechanical properties. Examples of the large anisotropy of piezoelectric coefficients, electromechanical coupling factors, squared figures of merit, and large hydrostatic parameters of the three-component 1–3-type composites are considered in the context of their piezotechnical applications. The applications of these materials include piezoelectric transducers, sensors, energy-harvesting and hydroacoustic devices.

1. Introduction

Composites based on ferroelectrics (FEs) are heterogeneous materials that belong to active dielectrics and form an important group of modern ‘smart materials’. This group is vast due to the large number of components that may be used in the composites that have a strong influence on their physical properties, electromechanical coupling and energy-harvesting characteristics. [1–5]. The piezo-active components which are often used to manufacture composites with predictable properties include FE ceramics and domain-engineered single crystals (SCs) [2–7] which exhibit important piezoelectric properties in their poled state. Undoubtedly, the piezoelectric properties and electromechanical coupling are of interest due to the opportunities to convert mechanical energy in electrical energy and vice versa [2 –4, 8]. This opens up a variety of possibilities to employ advanced piezo-active composites as elements for energy-harvesting devices [4, 9]. A number of piezo-active composites are of significant interest due to their ability to vary and tailor the microgeometry, effective piezoelectric properties, their anisotropy, hydrostatic, energy-harvesting and other parameters over a wide range [2 –5, 10].

The well-known classification of the two-component

[a] Prof. Dr. C. R. Bowen, Corresponding Author
Department of Mechanical Engineering
University of Bath
BA2 7AY Bath, United Kingdom
E-mail: c.r.bowen@bath.ac.uk
[b] Prof. Dr. V. Yu. Topolov
Department of Physics
Southern Federal University
5 Zorge street, 344090 Rostov-on-Don, Russia
[c] Dr. Y. Zhang
Department of Mechanical Engineering
University of Bath
E-mail: Y.Zhang2@bath.ac.uk
BA2 7AY Bath, United Kingdom
[d] Prof. Dr. A. A. Panich
Institute of High Technologies and Piezotechnics
Southern Federal University
10 Milchakov street, 344090 Rostov-on-Don, Russia

[a] Title(s), Initial(s), Surname(s) of Author(s) including Corresponding Author(s)
Department
Institution
Address 1
E-mail:
[b] Title(s), Initial(s), Surname(s) of Author(s)
Department
Institution
Address 2

Supporting information for this article is given via a link at the end of the document.((Please delete this text if not appropriate))

Christopher R. Bowen was born on January 18th, 1968 and grew up in Beddau, South Wales (UK). He earned a BSc (First Class) in Materials Science at the School of Materials, University of Bath, UK (1990) and worked on his DPhil thesis in the Department of Materials, University of Oxford, UK (PhD awarded in 1994). He joined the University of Bath, UK in 1998 and is now a Professor at the same University. His research interests are the manufacture and characterisation of ferroelectric ceramics and composites for sensor, actuator and energy-harvesting applications. Author of three monographs, over 250 papers, chapters in monographs, conference proceedings, and abstracts.

Vitaly Yu. Topolov was born in Rostov-on-Don (USSR, now Russia) on November 8th, 1961. He earned the qualification "Physicist. Educator" (honours degree, 1984) and degrees "Candidate of Sciences (Physics and Mathematics)" (1987) and "Doctor of Sciences (Physics and Mathematics)" (2000), all at the Rostov State University, Russia. Since 2006, he is a Professor of the Department of Physics at the Southern Federal University, Rostov-on-Don, Russia. Corresponding Member of the Russian Academy of Natural Science (Russia, 2010). His research interests include poludomain and heterophase ferroelectrics, smart materials and electromechanical effects in piezo-active composites. He is author of five monographs, three edited conference proceedings, and over 420 papers, chapters in monographs and reviews.

Yan Zhang was born in Fujian province, China on March 5th, 1986. She obtained her B.S., and PhD degrees in Materials Science at Central South University in China in 2008 and 2013, respectively. She then worked at the Hunan University in China for two years and from June 2016, she has been a Marie-Skłodowska-Curie Fellow at the University of Bath, UK. Her research interests concentrate on ferroelectric ceramics, bio-piezoelectric composites, porous structures, sensors and energy harvesting applications. She has published approximately 20 journal papers, received 14 awards, filed three patents with over 20 oral presentations at key conferences.

Alexander A. Panich was born in Rostov-on-Don (USSR, now Russia) on January 7th, 1972. He earned the qualification "Physicist" (1994) at the Rostov State University and degrees "Candidate of Sciences (Tech. Sci.)" (2003) and Doctor of Sciences (Tech. Sci.)" (2013). He is a Professor at the Institute of High Technologies and Piezotechnics at the Southern Federal University, Rostov-on-Don, Russia. His research interests include the elaboration of piezoelectric materials and devices. He is author of three monographs and over 80 papers, reviews, patents, conference proceedings, and abstracts.

---

composites was first put forward by Newnham *et al*. [11]. This classification is based on the concept of connectivity, and this concept has been developed in recent decades [3, 12]. Composite connectivity is regarded as one of the main characteristics of the composite and is expressed [1, 11] by the numbers of dimensions (or co-ordinate axes) in which each component is continuously distributed between limiting surfaces of the composite as a whole. The distribution of a self-connected state of a component can take place along zero, one, two, or three co-ordinate axes, i.e., connectivity α = 0, 1, 2, or 3 for the first component and connectivity β = 0, 1, 2, or 3 for the second component. A two-component composite is then described by α–β connectivity so that the connectivity of the piezoelectric (FE or most active component) takes the first position (α) [1–4, 11]. The concept of connectivity is highly useful in order to interpret the electromechanical interactions between individual components within piezo-active composites and to interpret experimental or predicted properties of composites with specific microgeometry [2, 3, 12]. The connectivity of the composite based a FE is crucial in influencing the piezoelectric response and electromechanical coupling [3, 11, 12]. Particular examples that have been experimentally studied in recent decades include composites with connectivities such as 1–3, 2–2, 0–3, 3–1, 3–2, and 3–3 [1–5, 9, 10]. In these composites at least one (first) component is FE and often influences the effective properties of the composite to a significant extent. In the case of the 1–3 composite shown in insets 1 and 2 in Fig. 1, the first (FE) component is distributed continuously along one co-ordinate axis (normally along the poling axis, as in OX_3 in Fig. 1), and the second component represents a matrix that is distributed continuously along three co-ordinate axes. A modification of the matrix and a formation of the composite structure therein (see insets 3–5 in Fig. 1) leads to changes in the effective properties of the composite that can be termed a '1–3-type composite'. These changes lead to the improvement of specific parameters of the 1–3-type composite [3–5, 13–17] in comparison to its conventional 1–3 equivalent.

This review paper is devoted to the effective properties and parameters of three-component 1–3-type composites based on FEs. Examples of the high performance of these composites are highlighted to demonstrate their applicability in piezoelectric transducer and energy-harvesting systems.

2. 1–3 Composites: Their Effective Properties and Related Parameters

The piezo-active 1–3 composites are widespread [1–5, 9–11, 13] due to their ease of poling and a variety of advantages over poled monolithic FE ceramics or SCs. The ceramic component can be represented by a continuous row of particles, relatively long rods or fibres, or a series of discs. The ceramic component can be surrounded by a matrix made of a range of materials such as a polymer or cement etc. [2, 18–20]. In Fig. 1, C1 is the main (FE) component with a high piezoelectric activity, and C2 is the matrix component that can be either piezoelectric or piezo-passive. The cross-section of the FE ceramic rod in the (X_1OX_2) plane (Fig. 1, insets 1 and 2) can be in the form of a circle, triangle, square, ellipse, etc. [13, 21]. In the 1–3 composite

based on FE SCs, the system of crystal rods that are poled along a specific crystallographic direction is often surrounded by a polymer matrix [9, 10]. A change of the poling direction in the SC rod leads to changes of its properties and, therefore, influences the effective properties, electromechanical coupling, piezoelectric anisotropy, hydrostatic and other parameters of the 1–3 composite [13, 22].

Our study is based on the model of a 1–3 composite that consists of a system of extended C1 rods aligned parallel to the poling axis OX_3. These rods are regularly distributed over a composite sample and surrounded by a continuous C2 matrix (see insets 1 and 2 in Fig. 1). We assume that a square arrangement of the rods is observed in the composite sample, i.e., the centres of symmetry of the base of the rods form a simple square lattice in the (X_1OX_2) plane shown in Fig. 1.

Hereafter the electromechanical properties of the C1 and C2 components are denoted with superscripts (1) and (2), respectively. The effective electromechanical properties of the 1–3 composite are determined in the long-wave approximation [3, 4] as a function of the volume fraction m of the C1 component by means of either the effective field method (for the circular cross section of the rod, see the inset 1 in Fig. 1) or matrix method (for the square cross section of the rod, see the inset 2 in Fig. 1) [3, 4, 13]. The long-wave approximation implies that the wavelength of an external acoustic field is much longer than the thickness of the individual rods in the 1–3 composite.

In the effective field method, elastic moduli $c_{ab}^{(n),E}$ measured at E = const, piezoelectric coefficients $e_{ij}^{(n)}$ and dielectric constants $\varepsilon_{pp}^{(n),\xi}$ measured at mechanical strain ξ = const are used to determine the effective electromechanical properties of the composite, i.e., the full set of c_{ab}^{*E}, e_{ij}^{*} and $\varepsilon_{pp}^{*\xi}$. According to the effective field method, the piezoelectric rods interact with the matrix when the composite is subjected to the action of an external electric and/or mechanical fields. Due to the presence of the ensemble of the similar rods in the matrix (see the inset 1 in Fig. 1), the field that acts on each rod can be regarded as an effective (or average) field [3, 13]. Such an effective field in the composite sample plays a key role in determining the effective electromechanical properties of the composite. These properties are determined from the matrix given by

$$|| C^{*} || = || C^{(2)} || + m (|| C^{(1)} || - || C^{(2)} ||) [|| I || + (1 - m) || S || \times \times || C^{(2)} ||^{-1} (|| C^{(1)} || - || C^{(2)} ||)]^{-1}. \quad (1)$$

In Eq. (1),

$$|| C^{(n)} || = \begin{pmatrix} || c^{(n),E} || & || e^{(n)} ||^{t} \\ || e^{(n)} || & - | \varepsilon^{(n),\xi} || \end{pmatrix} \quad (2)$$

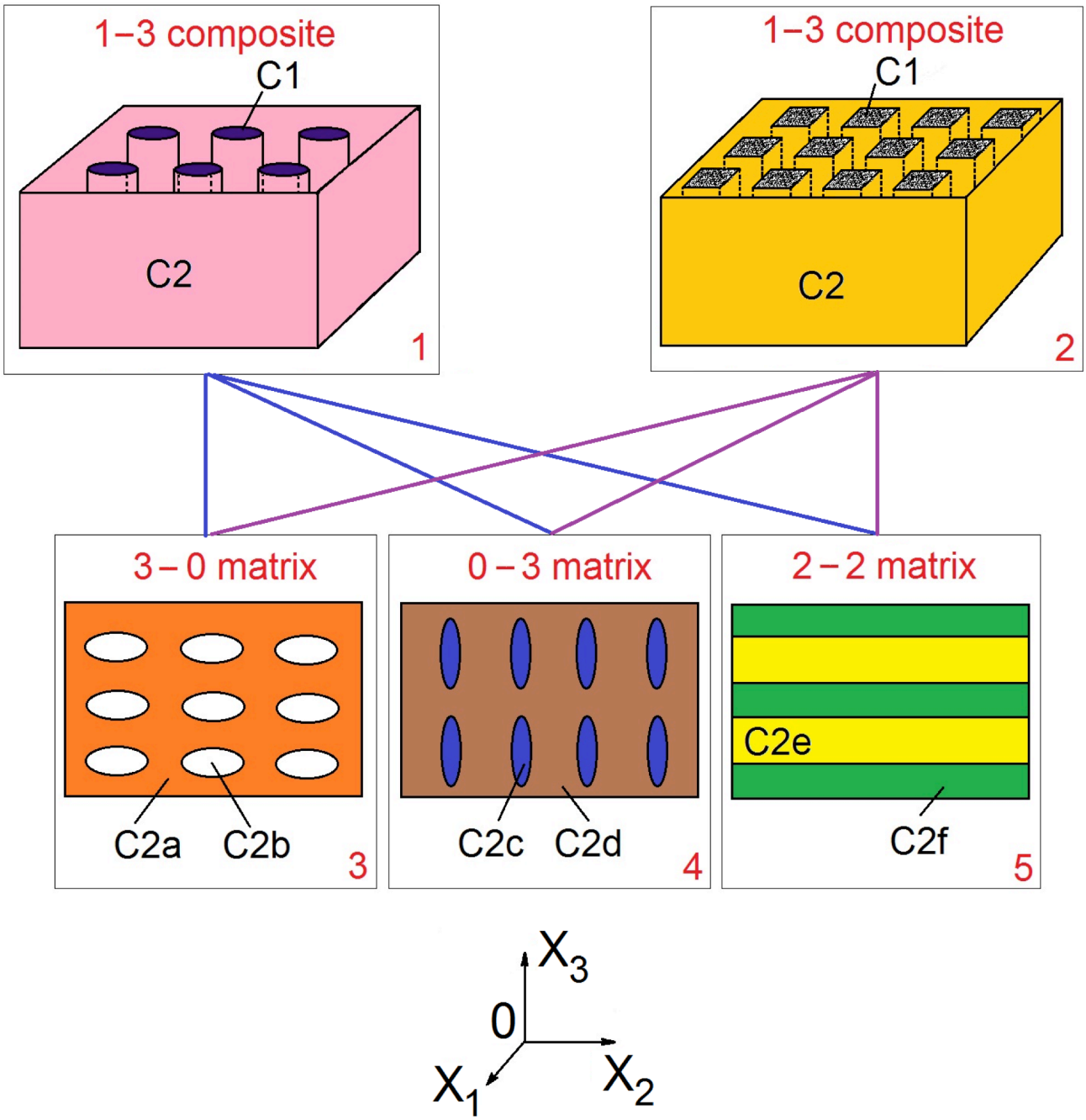

Figure 1. Schematic of a 1–3 composite (insets 1 and 2) and matrix (3–5). C1, C2, C2a, C2b, C2c, C2d, C2e, and C2f are components, and ($X_1X_2X_3$) is the rectangular co-ordinate system.

is a 9 × 9 matrix that characterises the electromechanical properties of the rods (n = 1) and the matrix (n = 2), || I || is a 9 × 9 identity matrix, || S || is a 9 × 9 matrix that contains components of the Eshelby electroelastic tensor [23]. In Eq. (2), superscript t denotes the transposition. The || C^* || matrix from Eq. (1) has a structure similar to that shown in Eq. (2).

electromechanical properties of the rod and the surrounding matrix in the OX_1 and OX_2 directions, in which the periodic structure of the composite is observed. Hereby the full sets of elastic compliances $s_{ab}^{(n),E}$ at E = const, piezoelectric coefficients $d_{ij}^{(n)}$ and dielectric permittivities $\varepsilon_{pp}^{(n),\sigma}$ at mechanical stress σ = const of the rod (n = 1) and the matrix (n = 2) are used.

The properties are averaged by taking into account boundary conditions [3, 13] for the electric and mechanical fields in the composite. The boundary conditions at interfaces x_f = const (f = 1 or 2, see the inset 2 in Fig. 1) indicate continuity of the three normal components of mechanical stress σ, three tangential

components of mechanical strain ξ, one normal component of electric displacement ***D***, and two tangential components of electric field ***E***. At the interface x_1 = const, the following components of the aforementioned fields are continuous: σ_{11}, σ_{12}, σ_{13}, ξ_{22}, ξ_{23}, ξ_{33}, D_1, E_2, and E_3. In the case of the interface x_2 = const, the following components are assumed to be continuous: σ_{12}, σ_{22}, σ_{23}, ξ_{11}, ξ_{13}, ξ_{33}, D_2, E_1, and E_3. The electromechanical properties of the *n*th component are given by a 9×9 matrix as follows:

$$|| C^{(n)}|| = \begin{pmatrix} || s^{(n),E} || & || d^{(n)} ||^t \\ || d^{(n)} || & || \varepsilon^{(n),\sigma} || \end{pmatrix} \quad (3)$$

In Eq. (3), $|| s^{(n),E} ||$ is the matrix of elastic compliances at E = const, $|| d^{(n)} ||$ is the matrix of piezoelectric coefficients, $|| \varepsilon^{(n),\sigma} ||$ is the matrix of dielectric permittivities at σ = const, and superscript *t* denotes the transposition. The effective electromechanical properties of the 1–3 composite shown in inset 2 in Fig. 1 are found in the long-wave approximation from the 9×9 matrix [3, 4, 13] given by

$$|| C^* || = [|| C^{(1)} ||\cdot|| M || m + || C^{(2)} || (1 - m)] [|| M || m + + || I || (1 - m)]^{-1}. \quad (4)$$

The structure of the $|| C^* ||$ matrix is similar to that shown in Eq. (3). In Eq. (4), *m* is the volume fraction of the C1 component, $|| I ||$ is the 9×9 identity matrix, and $|| M ||$ is the matrix concerned with the aforementioned boundary conditions at x_f = const (*f* = 1 and 2).

The effective properties calculated using the effective field method are compared to the effective properties calculated by means of the matrix method and finite element method [4, 5, 13, 21]. Based on the full set of electromechanical constants [i.e., elements of $|| C^* ||$ from Eq. (1) or (4)] and conventional formulae for the piezoelectric medium [8], we calculate the following effective parameters of the composite:

(i) piezoelectric coefficients d^*_{ij} and g^*_{ij} (hereby matrix relations

$$|| d^* || = || e^* ||\cdot|| c^{*E} ||^{-1} \text{ and } || d^* || = || \varepsilon^{*\sigma} ||\cdot|| g^* || \quad (5)$$

can be used),

(ii) longitudinal electromechanical coupling factor (ECF)

$$k^*_{33} = d^*_{33} / (\varepsilon^{*\sigma}_{33} s^{*E}_{33})^{1/2}, \quad (6)$$

transverse ECF

$$k^*_{31} = d^*_{31} / (\varepsilon^{*\sigma}_{33} s^{*E}_{11})^{1/2}, \quad (7)$$

thickness ECF

$$k^*_t = e^*_{33} / (\varepsilon^{*\xi}_{33} c^{*D}_{33})^{1/2}, \quad (8)$$

and planar ECF

$$k^*_p = k^*_{31}[2 s^{*E}_{11} / (s^{*E}_{11} + s^{*E}_{12})]^{-1/2}, \quad (9)$$

(iii) anisotropy factors

$$\zeta_d^* = d^*_{33} / d^*_{31}, \ \zeta_k^* = k^*_{33} / k^*_{31} = \zeta_d^* (s^{*E}_{11} / s^{*E}_{33})^{1/2} \text{ and } \zeta_{kt\text{-}p}^* = k^*_t / k^*_p, \quad (10)$$

(iv) squared figures of merit

$$(Q^*_{33})^2 = d^*_{33} g^*_{33} \text{ and } (Q^*_{31})^2 = d^*_{31} g^*_{31}, \quad (11)$$

(v) hydrostatic piezoelectric coefficients

$$d^*_h = d^*_{33} + d^*_{32} + d^*_{31} \text{ and } g^*_h = g^*_{33} + g^*_{32} + g^*_{31}, \quad (12)$$

(vi) hydrostatic squared figure of merit

$$(Q^*_h)^2 = d^*_h g^*_h, \quad (13)$$

and (vii) hydrostatic ECF

$$k^*_h = d^*_h / (\varepsilon^{*\sigma}_{33} s^{*E}_h)^{1/2}. \quad (14)$$

In Eq. (8), $\varepsilon^{*\xi}_{33} = \varepsilon^{*\sigma}_{33} - (d^*_{31} e^*_{31} + d^*_{32} e^*_{32} + d^*_{33} e^*_{33})$ is the dielectric permittivity at ξ = const, and $c^{*D}_{33} = c^{*E}_{33} / [1 - (k^*_t)^2]$ is the elastic modulus at D = const. The hydrostatic elastic compliance s^{*E}_h from Eq. (14) is written in terms of s^{*E}_{fp} [3, 26] as follows:

$s^{*E}_h = \sum_{f,p=1}^{3} s^{*E}_{fp}$. The hydrostatic parameters from Eqs. (12)–(14) are related to the composite sample with electrodes oriented perpendicular to the poling axis OX_3, see Fig. 1.

The piezoelectric coefficients d^*_{ij} and d^*_h are often used to describe piezoelectric activity of the composite, and the piezoelectric coefficients g^*_{ij} and g^*_h characterise its piezoelectric sensitivity [2–5]. The ECFs from Eqs. (6)–(9) and (14) are introduced to characterise an effectiveness of the conversion of mechanical energy into electric energy and vice versa at different oscillation modes and along fixed co-ordinate axes [8, 26, 27]. The anisotropy factors from Eqs. (10) characterise features of the piezoelectric (electromechanical) anisotropy of the composite sample at different oscillation modes [4, 13, 14]. The squared figures of merit from Eqs. (11) and (13) are related to power densities and signal-to-noise ratios in piezoelectric transducers, sensors, hydrophones, and other piezotechnical devices [3, 4, 27–30]. It is obvious that for energy-harvesting applications, the performance of a piezo-active composite depends on a set of its effective parameters that are to be chosen from Eqs. (6)–(14) in accordance with specific loading and oscillation modes.

Table 1 shows the FE and piezoelectric components that are of interest for our analysis for potential energy-harvesting applications of the composites based on these components. Table 2 shows the piezo-passive components examined in this work. In Table 1 we provide the full sets of electromechanical constants of the [001]-poled domain-engineered SCs and ceramics. Hereby the SCs can be divided into the following two groups:

(i) lead-containing relaxor-FE $(1 - x)Pb(Mg_{1/3}Nb_{2/3})O_3 - xPbTiO_3$ (PMN–*x*PT) and $(1 - x)Pb(Zn_{1/3}Nb_{2/3})O_3 - xPbTiO_3$ (PZN–*x*PT) with compositions near the morphotropic phase boundary and with the large piezoelectric coefficient $d_{33} > 10^3$ pC / N [6, 31–35], and

Table 1. Room-temperature elastic compliances s^E_{ab} (in 10^{-12} Pa^{-1}), piezoelectric coe domain-engineered SCs (4*mm* symmetry) and ceramics (∞*mm* symmetry)

FE components	s^E_{11}	s^E_{12}	s^E_{13}	s^E_{33}	s^E_{44}	
						Lead-containing relaxor-F
PMN–0.33PT [6]	69.0	–11.1	–55.7	119.6	14.5	
PMN–0.30PT [31]	52.0	–18.9	–31.1	67.7	14.0	
PMN–0.29PT [32]	52.1	–24.6	–26.4	59.9	16.0	
PMN–0.28PT [33]	44.57	–28.91	–13.91	34.38	15.22	1
PZN–0.045PT [34]	82.0	–28.5	–51.0	108	15.6	
PZN–0.07PT [35]	85.9	–14.1	–69.0	142	15.9	
PZN–0.08PT [35]	87.0	–13.1	–70.0	141	15.8	
						Lead-free FE SCs
KNN–T[a]	11.9	–4.30	–5.60	15.5	12.0	
KNN–TL[b]	17.2	–5.11	–10.7	27.0	15.4	

Table 2. Room-temperature elastic compliances s_{ab} (in 10^{-12} Pa^{-1}) and dielectric permittivity ε_{pp} of piezo-passive polymers

Polymer components	s_{11}	s_{12}	ε_{pp} / ε_0
Araldite [24]	216	–78	4.0
Polyurethane [26]	405	–151	3.5
Elastomer [40]	3300	–1480	5.0
Monolithic polyethylene [41, 42]	1430	–286	2.3
Auxetic polyethylene [41, 42]	5260	4360	2.3

(ii) lead-free FE SCs based on alkali niobates with the moderate piezoelectric coefficient $d_{33} \sim 10^2$ pC / N and large piezoelectric coefficient $g_{33} \approx$ 50–100 mV·m / N [7, 36, 37].

The piezoelectric coefficient d_{33} of the poled FE ceramics [3, 4, 13, 28, 38, 39] can be either comparable to the d_{33} values of lead-free SCs (see PCR-7M or PZT-5H in Table 1) or smaller than the d_{33} of the lead-free SCs (see modified $PbTiO_3$ in Table 1).

Data on polymers in Table 2 suggest that the elastic properties of these isotropic components vary in a wide range. Among them, of specific interest is auxetic polyethylene with a negative Poisson's ratio [41].

Examples of the piezoelectric performance and figures of merit of the 1–3 ceramic / polymer composites are shown in Table 3. An important feature of the 1–3 composites based on

Table 3. Piezoelectric coefficient d_{33}^* (in pC / N), piezoelectric anisotropy factor ζ_d* and squared figures of merit $(Q_{3j}^*)^2$ (in 10^{-12} Pa^{-1}) of the 1–3 PCR-7M ceramic / polymer composite[a]

Polymer components	m	d_{33}^*	ζ_d*	$(Q_{33}^*)^2$	$(Q_{31}^*)^2$
Araldite	0.05	279	–2.65	59.3	8.42
	0.10	418	–2.62	55.9	8.13
	0.20	557	–2.56	42.5	6.50
	0.30	627	–2.50	33.5	5.36
	0.50	697	–2.38	23.2	4.08
Polyurethane	0.05	396	–2.60	102	15.1
	0.10	529	–2.57	78.8	11.9
	0.20	637	–2.52	51.2	8.09
	0.30	683	–2.46	37.6	6.20
	0.50	725	–2.36	24.5	4.38
Elastomer	0.05	683	–2.22	222	44.8
	0.10	721	–2.22	121	24.5
	0.20	742	–2.21	63.0	12.8
	0.30	750	–2.21	42.6	8.73
	0.50	756	–2.20	25.9	5.36
Auxetic polyethylene	0.05	652	1.89	211	59.1
	0.10	693	2.60	115	17.0
	0.20	721	5.63	69.7	1.92
	0.30	733	38.9[b]	41.5	0.0274
	0.50	746	–5.37	25.5	0.884

[a] See the inset 2 in Fig. 1, where C1 is the FE ceramic component (volume fraction m), and C2 is the polymer component (volume fraction 1 – m)
[b] $d_{31}^* = 0$ and $(Q_{31}^*)^2 = 0$ at $m = 0.320$

FEs [3–5, 26] consists in the piezoelectric coefficients d_{3j}^* that obey the conditions,

$$d_{33}^* >> d_{15}^* \text{ and } |d_{31}^*| >> d_{15}^* \quad (15)$$

in wide volume-fraction (m) ranges. The validity of the conditions (15) is caused by the composite architecture (see insets 1 and 2 in Fig. 1). In such a composite system, the shear piezoelectric activity is strongly suppressed by the system of parallel FE rods poled along the OX_3 axis. Hereafter we do not consider the shear piezoelectric effect and related parameters of the composites in the present paper. We add that due to the same system of the FE rods, the piezoelectric coefficient $d_{33}^*(m)$ increases monotonously on increasing the volume fraction of FE m. As seen from Table 3, the softer polymer matrix promotes a larger $d_{33}^*(m)$ value and does not lead to considerable changes of the anisotropy factor ζ_d*(m) in the case of a conventional polymer component with a positive Poisson's ratio. The auxetic polymer component influences the $d_{3j}^*(m)$ and ζ_d*(m)

dependences to a certain degree. Due to the elastic properties of the auxetic polymer matrix, the sign of the piezoelectric coefficient d_{31}^* changes at a volume fraction $m = m^*$, and therefore, conditions

$$\zeta_d^* \to \pm\infty,\ \zeta_k^* \to \pm\infty \text{ and } \zeta_{kt\text{-}p}^* \to \pm\infty \qquad (16)$$

hold at $m = m^*$. Since Eqs. (7) and (9) hold, the ECFs k_{31}^* and k_p^* pass the zero value at the same volume fraction m^*, and $k_{33}^* \neq 0$ and $k_t^* \neq 0$ due to inequalities $d_{33}^* \neq 0$ and $e_{33}^* \neq 0$ at $m = m^*$ [see also Eqs. (6) and (8)]. As is known from numerous papers [3–5, 13, 17, 25, 40] on the piezo-active 1–3 composites poled along the OX_3 axis, their piezoelectric coefficients d_{33}^* and e_{33}^* demonstrate a monotonic increase at $0 < m < 1$. Large absolute values of the anisotropy factors from (16) are beneficial for piezoelectric energy-harvesting devices [4]: in this case we have the preferential direction of the energy conversion (OX_3) at specific oscillation modes of the piezoelectric element, i.e., the longitudinal mode concerned with the ECF k_{33}^* or the thickness mode concerned with the ECF k_t^*. For a large piezoelectric anisotropy, the transverse oscillation mode concerned with d_{31}^* does not play an important role in the energy conversion, and vibration harvesting can take place along the poling axis OX_3 of the composite sample.

Examples of the large piezoelectric anisotropy and validity of conditions (16) in composites with auxetic polymer matrices were discussed in work [4, 17, 43]. Of particular interest are the lead-free composites [43] where the SC rods are based on FE lead-free (K, Na)(Nb, Ta)O_3 and (Li, K, Na)(Nb, Ta)O_3 solid solutions, and the auxetic polyethylene matrices (PE-*n* where *n* = 1, 2, …, 9) are characterised by Poisson's ratios [41] from –0.83 to –0.29. It is assumed that the SC rods are in the form of the rectangular parallelepiped with a square base (see the inset 2 in Fig. 1), and the surrounding auxetic matrix is regarded as a continuous isotropic medium without a specification of its microstructure. This approximation enables us to characterise the composite from work [43] by 1–3 connectivity. The main crystallographic axes *X*, *Y*, and *Z* of each SC rod are parallel to the following co-ordinate axes: *X* || OX_1, *Y* || OX_2 and *Z* || OX_3, and the spontaneous polarisation vector of each SC rod is $\boldsymbol{P_s}^{(1)} \uparrow\uparrow OX_3$. This means that we consider a case of the [001]-poled composite with a piezo-passive matrix.

Nine examples of the auxetic polyethylene matrices [41] with *n* = 1, 2, …, and 9 have been considered [43] to compare with the piezoelectric performance of lead-free 1–3 composites. These materials exhibit advantageous properties over numerous lead-based piezo-active composites and ceramics [2–5, 9, 10, 22, 24, 25]. We mention the high longitudinal piezoelectric coefficient $g_{33}^* \sim (10^2\text{–}10^3)$ mV·m / N and squared figure of merit $(Q_{33}^*)^2 \sim 10^{-11}$ Pa^{-1}, as well as hydrostatic piezoelectric coefficient $g_h^* \sim (10^2\text{–}10^3)$ mV·m / N and squared figure of merit $(Q_h^*)^2 \sim (10^{-11}\text{–}10^{-10})$ Pa^{-1}, see examples in Fig. 2. We consider cases of the volume fraction of SC $m = 0.05$ and 0.10: at these volume fractions, the piezoelectric sensitivity and squared figures of merit remain relatively large despite maxima of g_{33}^* and g_h^* in the range $0 < m < 0.03$. In the studied composites, an infinitely large anisotropy and validity of conditions (16) are observed, and the volume fraction m^* related to $d_{31}^* = 0$ strongly depends on the elastic properties of the auxetic polymer component. According to data [43], $m^* \approx 0.2\text{–}0.3$ for the composites based on the KNN-TL and KNN-T SCs. Due to the 1–3 composite structure shown in the inset 2 in Fig. 1, the condition $k_t^* = k_{33}^*$ is valid with an accuracy to 3% at a volume fraction $m = m^*$ [43]. It is important to underline that the values of the squared figure of merit $(Q_{33}^*)^2$ of the lead-free 1–3 composites (Fig. 2) are larger than $(Q_{33}^*)^2$ of the 1–3 PCR-7M ceramic / auxetic polyethylene composite (see Table 3) even in the volume-fraction range where the condition

$$(Q_{33}^*)^2 / (Q_{31}^*)^2 >> 1 \qquad (17)$$

holds. It should be added that the g_h^* values shown in Fig.2 are approximately 5–16 times more than the max g_h^* of the 1–3 PMN–*x*PT SC / araldite and PZN–*x*PT SC / araldite composites [3], and the $(Q_h^*)^2$ values from Fig. 2 are 20–43 times more than values of max[$(Q_h^*)^2$] of the aforementioned lead-based 1–3 composites [3]. As follows from data [10] for a 1–3 PMN–0.30PT SC / epoxy composite, its max $g_{33}^* = 440$ mV·m / N is achieved at a volume fraction of SC $m = 0.018$ and approximately 1.3–1.5 times smaller than g_{33}^* of the lead-free 1–3 SC / auxetic polyethylene composites, see Fig. 2.

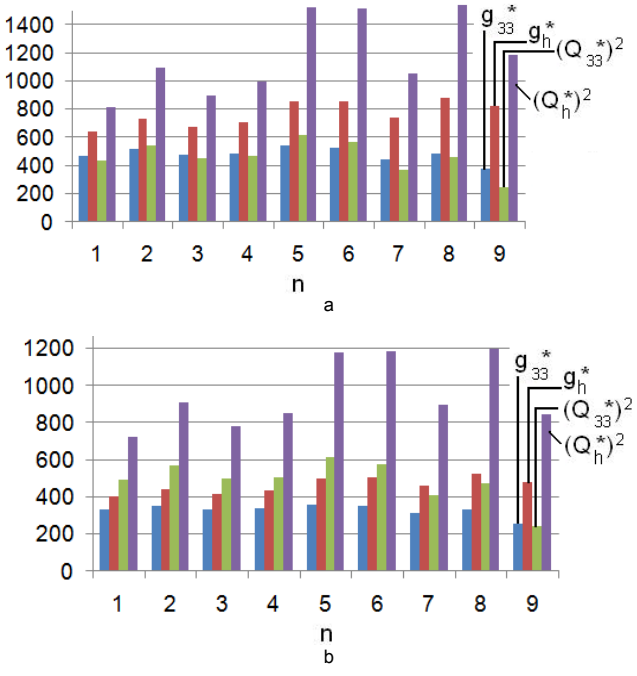

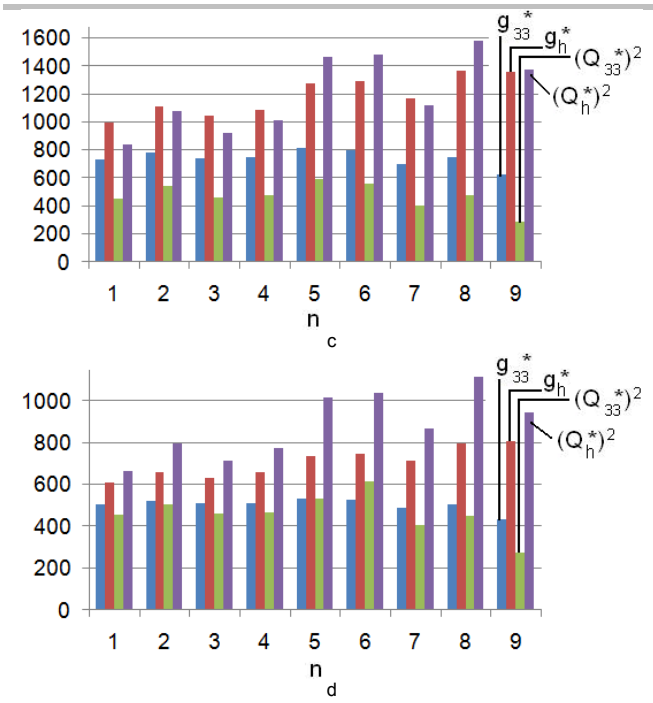

Figure 2 (continued)

Figure 2. Piezoelectric coefficients g_{33}^* and g_h^* (in mV·m / N) and squared figures of merit $(Q_{33}^*)^2$ and $(Q_h^*)^2$ (in 10^{-13} Pa^{-1}) of 1–3 KNN-TL SC / auxetic PE-*n* (a and c) and KNN-T SC / auxetic PE-*n* (b and d) composites at volume fractions of SC *m* = 0.05 (a and b) and *m* = 0.10 (c and d) (reprinted from paper by Topolov and Bowen [43], with permission from Elsevier)

3. 1–3-Type Composites: Improving Effective Parameters

A large number of possibilities exist to modify the polymer matrix surrounding the FE rods in 1–3-type composite (see insets 3 –5 in Fig. 1). This can lead to an improvement in composite performance including the piezoelectric anisotropy, sensitivity, squared figures of merit, electromechanical coupling factors, and hydrostatic parameters [3–5, 14–16, 26]. In Section 3 we discuss examples of the 1–3-type composites based on FEs to show the important role of the matrix in forming the piezoelectric response and highlight methods for improving the effective parameters of the composites.

3.1. Piezoelectric Anisotropy

An important stimulus is to improve the piezoelectric anisotropy and to achieve a larger $|\zeta_d^*|$ for transducer and energy-harvesting applications of 1–3-type composites [1–4]. One solution to this problem is related to a 1–3–0 composite [3, 4, 14] wherein the matrix surrounding the FE rods represents a porous polymer medium.

It is assumed that the 1–3–0 composite contains a system of parallelepipedic SC rods in a porous polymer matrix (see insets 2 and 3 in Fig. 1). As discussed earlier, the SC rods have a square base and are characterised by a periodic square arrangement in the (X_1OX_2) plane. The main crystallographic axes *X*, *Y*, and *Z* of the SC rod are parallel to the co-ordinate axes OX_j as follows: X || OX_1, Y || OX_2 and Z || OX_3, and the spontaneous polarisation vector of the rod is $\boldsymbol{P}_s^{(1)} \uparrow\uparrow OX_3$. The porous polymer matrix that surrounds the rods contains a system of spheroidal air pores (see C2b in the inset 3 in Fig. 1) that are described by the equation

$$(x_{1,p} / a_1)^2 + (x_{2,p} / a_1)^2 + (x_{3,p} / a_3)^2 = 1 \qquad (18)$$

relative to the axes of the rectangular co-ordinate system $(X_1X_2X_3)$. Semi-axes of the spheroidal pore from Eq. (18) equal $a_{,p\,1}$, $a_{2,p} = a_{1,p}$ and $a_{3,p}$. The porous matrix is characterised by 3–0 connectivity, see the inset 3 in Fig. 1. The pores are regularly distributed in the polymer matrix and occupy sites of a simple tetragonal lattice. The shape of each pore is characterised by an aspect ratio $\rho_p = a_{1,p} / a_{3,p}$ that is fixed over the composite sample. The radius or the largest semi-axis (for instance, $a_{1,p} = a_{2,p}$ for the oblate pore) remains much smaller than the length of the side of the square that is the intersection of the SC rod by the (X_1OX_2) plane.

The effective electromechanical properties of the 1–3–0 composite are evaluated as follows [3–5, 14]. In the first stage, the effective properties of the piezo-passive polymer matrix with aligned spheroidal pores are determined [14, 44] as a function of the volume fraction of the pores (or porosity of the polymer matrix) m_p and the aspect ratio ρ_p. The corresponding calculation procedure is based on Eshelby's concept [23, 44] of spheroidal inclusions in heterogeneous solids. The effective properties of the porous medium (3–0 composite) shown in the inset 3 in Fig. 1 are given by [4, 14, 44]

$$|| C^{(3\text{-}0)} || = || C^{(pol)} ||\cdot[|| I || - m_p(|| I || - (1 - m_p)|| S ||)^{-1}]. \qquad (19)$$

In Eq. (19), $|| C^{(pol)} ||$ is a 9 × 9 matrix of the properties of the polymer component (see C2a in the inset 3 in Fig. 1), $|| I ||$ is 9 × 9 identity matrix, and $|| S ||$ is the 9 × 9 matrix that comprises components of the electroelastic Eshelby tensor. We add that elements of the $|| S ||$ matrix depend on the aspect ratio ρ_p of the pore and on the properties of the polymer component [23]. In the second stage, the effective properties of the 1–3–0 composite are evaluated using Eq. (4) and take into account the properties of the SC rod [$|| C^{(1)} ||$ in Eq. (4)] and porous polymer matrix for which the equality $|| C^{(2)} || = || C^{(3\text{-}0)} ||$ now holds. The averaging procedure enables us to find the effective electromechanical properties of the 1–3–0 composite $\Pi^* = \Pi^*(m, m_p, \rho_p)$.

In the case of the 1–3–0 composite based on a PMN–0.33PT SC (Fig. 3), we state consider the influence of the porous 3–0 matrix on the anisotropy factor ζ_d^*. A strong influence is observed in the presence of a matrix with heavily oblate pores, i.e., at ρ_p = 100, see curves 4–6 in Fig. 3. An increase of porosity m_p in the polymer matrix promotes a larger $|\zeta_d^*|$ value (cf. curves 4 and 6 in Fig. 3). A decrease of the aspect ratio ρ_p at m_p = const (see curves 4, 3 and 2 in Fig. 3) leads to a smaller $|\zeta_d^*|$ value. Such a behaviour of

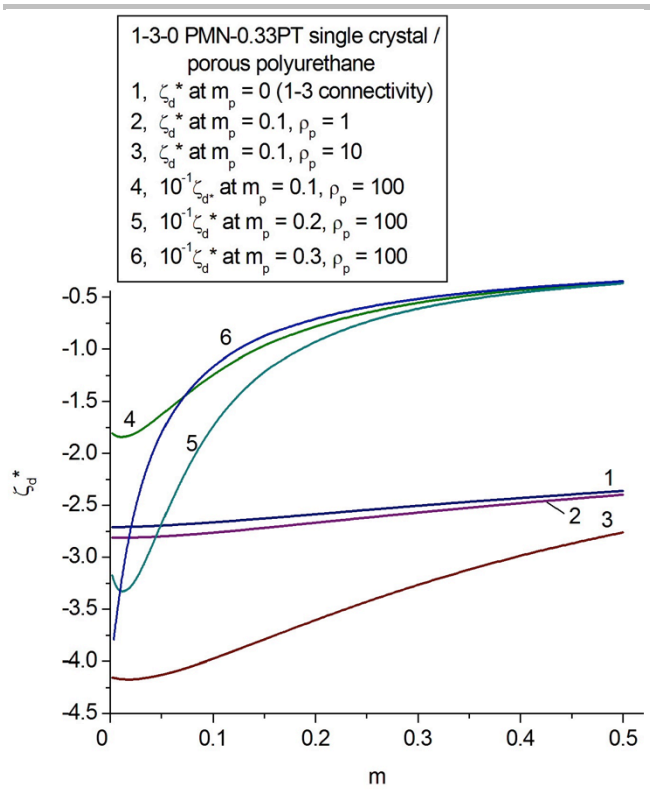

Figure 3. Piezoelectric anisotropy factor ζ_d^* of the 1–3–0 PMN–0.33PT SC / porous polyurethane composite

the anisotropy factor ζ_d^* enables us to emphasise the important role of the elastic anisotropy of the porous 3–0 matrix in forming the piezoelectric anisotropy in the 1–3–0 composite. As follows from our evaluations [14] of the elastic compliances $s_{ab}^{(3-0)}$ of the porous matrix, the small anisotropy (i.e., $s_{11}^{(3-0)} / s_{33}^{(3-0)} \approx 1$) is observed at $\rho_p < 1$ and partially at $\rho_p > 1$ (as a rule, at porosity $m_p < 0.2$). The formation of highly oblate pores at $\rho_p >> 1$ and increasing porosity m_p lead to the ratio $s_{11}^{(3-0)} / s_{33}^{(3-0)} >> 1$ that leads to large $|\zeta_d^*|$ values in the composite, We note that a large piezoelectric anisotropy at $m > 0.05$ is achieved for a piezoelectric coefficient $d_{33}^* > 1500$ pC / N [5] due to the very high piezoelectric coefficient d_{33} of the SC, see Table 1.

An important example of the piezoelectric anisotropy is reported for a 1–2–2 composite. It is assumed that its SC rods have a square base and are characterised by a periodic square arrangement in the (X_1OX_2) plane. They are surrounded by a 2–2 laminar matrix that is shown in inset 5 of Fig. 1. The polymer layers in this matrix (C2e and C2f in the inset 5 in Fig. 1) are regularly distributed along the OX_3 axis and separated by planar interfaces parallel to the (X_1OX_2) plane. Hereafter we assume that the polymer component with a high stiffness is characterised by a volume fraction m_s, and the component with a smaller stiffness is characterised by a volume fraction $1 - m_s$. In the first stage of our evaluations, the effective properties of the 2–2 matrix are found by means of the matrix method [3, 4, 13, 24, 25], see Eq. (4). The boundary conditions for electric and mechanical fields are applied to the interfaces $x_3 = \text{const}$ shown in the inset 5 in Fig. 1. In the second stage, an averaging procedure is performed within the framework of the same method, but for a system of "SC rods – laminar polymer matrix", and the boundary conditions are applied to the interfaces $x_1 = \text{const}$ and $x_2 = \text{const}$ (see inset 2 in Fig. 1). Hereby we assume that the thickness of each polymer layer of the 2–2 matrix is much smaller than the linear sizes of the SC rod base in the (X_1OX_2) plane, i.e., the system of the SC rods is surrounded by a heterogeneous polymer matrix with the effective properties that have been determined in the first stage. Finally, the effective electromechanical properties of the 1–2–2 composite are represented as $\Pi^* = \Pi^*(m, m_s)$. Among the properties we consider the piezoelectric coefficients that obey the following condition for the large anisotropy:

$$|\zeta_d^*| \geq 5. \tag{20}$$

The condition (20) for the 1–2–2 composite holds at

$$m_{d,1} \leq m \leq m_{d,2} \tag{21}$$

and $m_s = \text{const}$. In Fig. 4 we show the areas where the condition (20) holds: the area between curves 1 and 2 is related to the polyurethane-containing composite, and the area between curves 1 and 3 is related to the araldite-containing composite. As follows from Table 2, the larger difference between the elastic compliances of the polymer components s_{ab} is observed in the araldite / polyethylene matrix. This promotes validity of the inequalities $s_{11}^{(2-2)} / s_{33}^{(2-2)} >> 1$ for the laminar matrix and (20) for the 1–2–2 composite in the larger area between curves 1 and 3 in Fig. 4.

Now we compare the piezoelectric performance of the 1–2–2 KNNTL:Mn SC / araldite / polyethylene composite at $m = 0.20$ and $m_s = 0.50$ (see the area between curves 1 and 3 in Fig. 4) to

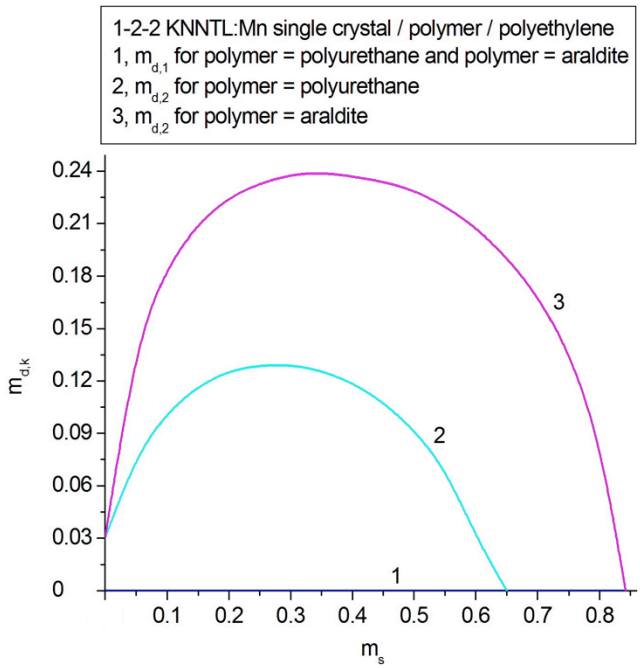

Figure 4. Bounds for the volume fraction of SC $m_{d,k}$ from the in equation (21) for the 1–2–2 KNNTL:Mn SC / polymer / polyethylene composite. m_s is the volume fraction of either polyurethane (1–2–2 KNNTL:Mn SC / polyurethane / polyethylene composite) or araldite (1–2–2 KNNTL:Mn SC / araldite / polyethylene composite).

the performance of the 1–2–2 KNNTL:Mn SC / polyurethane / polyethylene composite at $m = 0.10$ and $m_s = 0.30$ (see the area between curves 1 and 2 in Fig. 4). According to our results, the aforementioned araldite-containing composite is characterised

by piezoelectric coefficients d_{33}^* = 414 pC / N and g_{33}^* = 449 mV·m / N, and its polyurethane-containing counterpart is characterised by d_{33}^* = 367 pC / N and g_{33}^* = 860 mV·m / N. The smaller volume fraction of SC *m* promotes the larger g_{33}^* value mainly due to the smaller dielectric permittivity $\varepsilon_{33}^{*\sigma}$. The value of g_{33}^* = 860 mV·m / N is approximately nine times larger than g_{33} of the KNNTL:Mn SC [7]. Such a performance of the 1–2–2 composite can be accounted for by the moderate dielectric permittivity $\varepsilon_{33}^{\sigma}$ of the KNNTL:Mn SC: its value is about 12.6 times smaller than $\varepsilon_{33}^{\sigma}$ of the PMN–0.33PT SC, see Table 1.

3.2. Electromechanical Coupling Factors

The 1–2–2 composites based on the KNNTL:Mn SC are also of interest due to the anisotropy of the ECFs from Eqs. (6)–(9). Fig. 5 show that conditions for the large anisotropy (20) and

$$|\zeta_k^*| \geq 5 \text{ and } |\zeta_{kt\text{-}p}^*| \geq 5 \qquad (22)$$

are valid in specific volume fractions ranges of *m* and m_s. Due to the links between the anisotropy factors (10) and elastic compliances s_{ab}^{*E} of the composite, changes in the volume fractions *m* and m_s lead to changes in the elastic properties of the laminar matrix and composite, especially when *m* << 1. Minima of the ECFs ζ_k^* and $\zeta_{kt\text{-}p}^*$ are observed in Fig. 5 at relatively small volume fractions *m*, when the laminar matrix plays an important role in forming the piezoelectric response of the composite. The relatively small difference between the elastic properties of polyurethane and polyethylene leads to a small difference (less than 3%) between the anisotropy factors ζ_d^* at m_s = 0.10–0.30. As a result of this small difference, in Fig. 5, b we omit the ζ_d^* curve related to m_s = 0.30.

A simultaneous validity of conditions (20) and (22) for the large piezoelectric anisotropy and anisotropy of ECFs, respectively, is observed in the araldite-containing composite, see curves 1–3 and 4–6 in Fig. 5, c and curves 1–3 in Fig. 5, d. However Fig. 5, d suggests that an increase of the volume fraction of araldite (m_s > 0.20) does not promote validity of conditions (20) and (22), see curves 4–6. This is concerned with the active role of the elastic properties of the laminar matrix in forming the piezoelectric anisotropy at relatively small volume fractions of SC *m*.

Large values of the thickness ECF 0.9 < k_t^* < 0.95 (Fig. 6) are achieved at small volume fractions of SC *m* and undergo minor changes on variation of the volume fraction of araldite m_s. This is due to the relatively small dielectric permittivity $\varepsilon_{33}^{*\xi}$ and elastic modulus c_{33}^{*D} which are related to the longitudinal response of the composite. It is seen from Eq. (8) that the relations $k_t^* \sim e_{33}^*$ and $k_t^* \sim 1/(\varepsilon_{33}^{*\xi} c_{33}^{*D})^{1/2}$ hold simultaneously. As a consequence, a compromise takes place when the ECF k_t^* reaches a large values at *m* < 0.1, i.e., at a small piezoelectric coefficient e_{33}^* that undergoes an almost linear increase in this volume-fraction (*m*) range. However at *m* < 0.1 irrespective of m_s, the elastic properties of the laminar matrix play the dominant

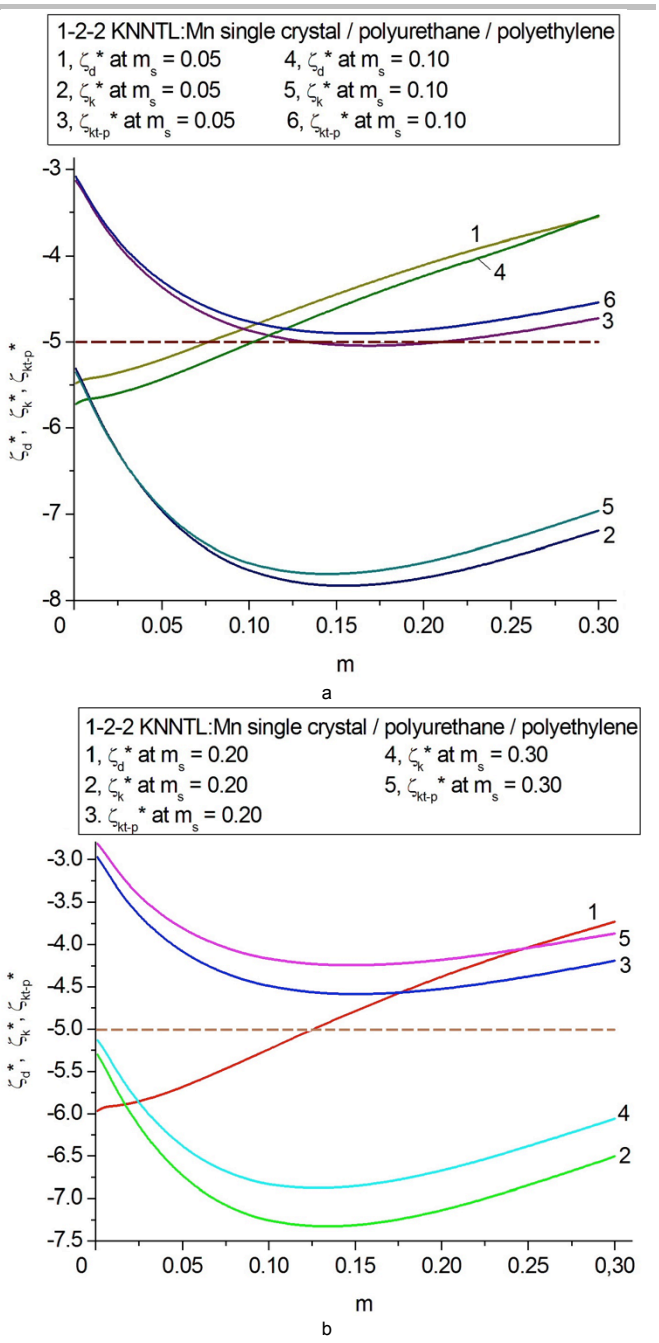

Figure 5. Anisotropy factors (10) of the 1–2–2 KNNTL:Mn SC / polymer / polyethylene composite. m_s is the volume fraction of either polyurethane (KNNTL:Mn SC / polyurethane / polyethylene composite, graphs a and b) or araldite (KNNTL:Mn SC / araldite / polyethylene composite, graphs c and d). The dotted line $\zeta_d^* = \zeta_k^* = \zeta_{kt\text{-}p}^* = -5$ is drawn for eye guide

role in forming the ECF k_t^* and remains comparable to the elastic properties of the 1–2–2 composite.

3.3. Squared Figures of Merit

As is known from work [3–5, 13–16, 26, 45, 46], the modification of the polymer matrix surrounding the FE rods in the 1–3-type composite influences its squared figures of merit $(Q_{3j}^*)^2$ from Eqs. (11) and anisotropy of $(Q_{3j}^*)^2$. These parameters are often used to characterise the sensor signal-to-noise ratio of a piezoelectric element and its sensitivity [3, 4, 28–30]. In some cases the

modification of the polymer matrix in the composite (see insets 3–5 in Fig. 1) leads to a larger piezoelectric anisotropy, and $|\zeta_d^*|$ increases. Due to this increase, a larger ratio of the squared figures of merit $(Q_{33}^*)^2/(Q_{31}^*)^2 = (\zeta_d^*)^2$ is expected. This facilitates energy conversion along the poling direction OX_3 in the composite. The piezoelectric element with a large $(Q_{33}^*)^2$ value will generate a high voltage and power during the longitudinal oscillation mode, and this is important in piezoelectric energy-harvesting and sensor applications [28–30]. In Section 3.3 we highlight examples of the behaviour of the squared figures of merit $(Q_{3j}^*)^2$ in the 1–3-type composites.

The first example is concerned with a 1–3–0 PMN–0.28PT SC / porous araldite composite that contains a system of parallelepipedic SC rods in a porous polymer matrix (see the description in the first part of Section 3.1 and insets 2 and 3 in Fig. 1). Hereby we consider the PMN–0.28PT SC as a main FE component with a small piezoelectric anisotropy (d_{33} / d_{31} = –2.08) and relatively small squared figure of merit ($d_{33}g_{33}$ = 28.8·10^{-12} Pa^{-1} in accordance with data from Table 1). We observe large values of $(Q_{33}^*)^2$ and validity of the condition (17) for the 1–3–0 PMN–0.28PT-based composite, see Fig. 7. Maxima of $(Q_{3j}^*)^2$ are achieved at volume fractions of SC m < 0.1, and this is accounted for by the strong influence of the dielectric permittivity $\varepsilon_{33}^{*\sigma}$ on the squared figures of merit. We remind the reader that in accordance with Eqs. (5), the squared figures of merit $(Q_{3j}^*)^2$ these 1–3-type composites can be represented as $(Q_{3j}^*)^2 = (d_{3j}^*)^2 / \varepsilon_{33}^{*\sigma}$. A competition between the increasing piezoelectric coefficient $|d_{3j}^*|$ and dielectric permittivity $\varepsilon_{33}^{*\sigma}$ leads to a compromise when max$[(Q_{3j}^*)^2]$ is achieved. The porous polymer matrix (see the inset 3 in Fig. 1) is characterised by anisotropic elastic properties which impedes the transverse piezoelectric effect in the 1–3–0 composite which becomes more appreciable at pore aspect ratios ρ_p >> 1, i.e., in the presence of heavily oblate pores in the polymer matrix. Comparing the graphs in Fig. 7, we note that a larger $(Q_{33}^*)^2$ value is achieved on increasing ρ_p (at m_p = const) and m_p (at ρ_p = const). However maximum points of $(Q_{33}^*)^2$ shift towards smaller volume fractions m on increasing ρ_p, cf. Fig. 7, c and 7, b. This is directly linked to the elastic anisotropy of the porous 3–0 matrix surrounding the SC rods: as is known from Section 3.1, the condition $s_{11}^{(3-0)}/s_{33}^{(3-0)}$ >> 1 holds for the elastic compliances of this matrix at ρ_p >> 1. Here we mention that Choy et al. [47] manufactured a 1–3 ceramic / polymer composite with a ceramic rod volume fraction of $m \approx 0.033$, 0.066, etc., and hence it is possible to solve the technological challenges and manufacture the 1–3-type composites in the vicinity of max$[(Q_{3j}^*)^2]$.

The validity of condition (20) favours a considerable hydrostatic piezoelectric response for the composite. One can observe a correlation between a large $(Q_{33}^*)^2$ value and large hydrostatic squared figure of merit $(Q_h^*)^2$, see Fig. 7. This becomes very distinct in the presence of a porous matrix at ρ_p = 100, see curves 1 and 3, 4 and 6, 7 and 9 in Fig. 7, c. We add that some features of the hydrostatic piezoelectric response of

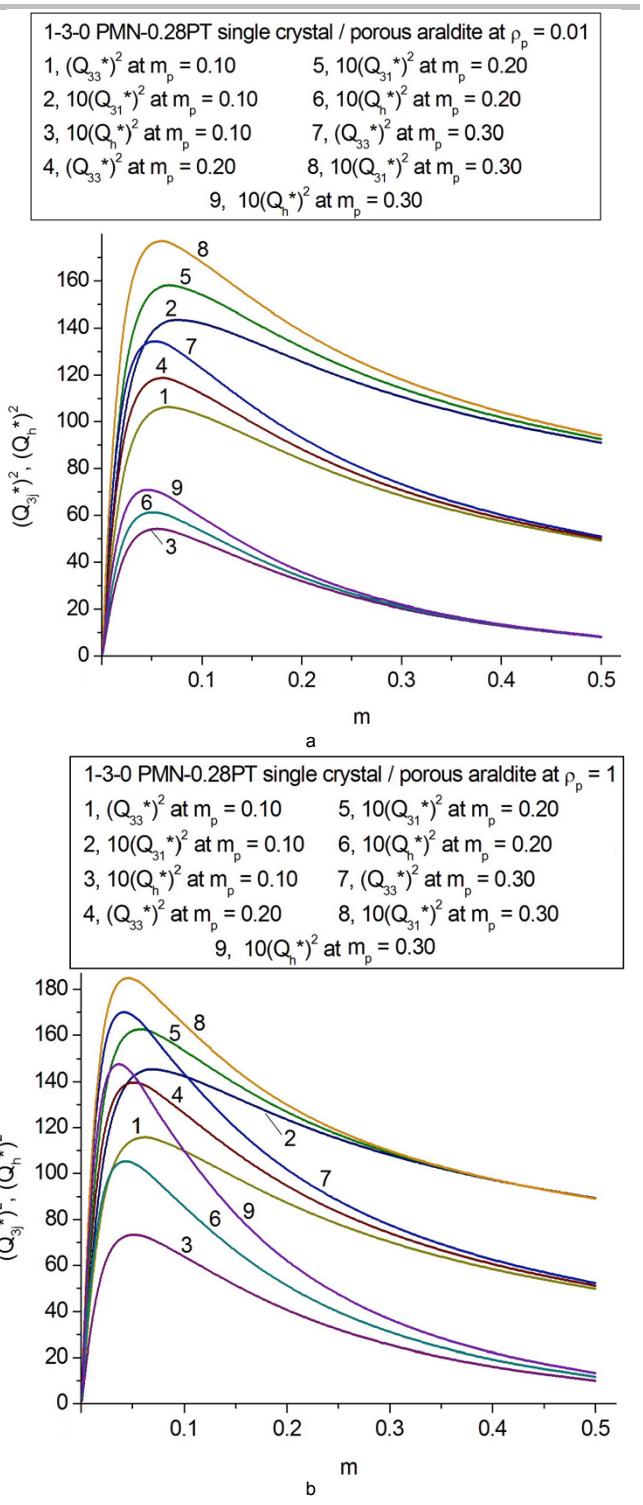

Figure 7. Squared figures of merit $(Q_{3jt}^*)^2$ and $(Q_h^*)^2$ (in 10^{-12} Pa^{-1}) of the 1–3–0 PMN–0.28 PT SC / porous araldite composite

the 1–3-type composites will be considered in Section 3.4.

The next example of the behaviour of $(Q_{3j}^*)^2$ is concerned with a 1–0–3 composite based on the PMN–0.33PT SC [45]. It is assumed that the 1–0–3 composite consists of long SC rods embedded in a 0–3 ceramic / polymer matrix (see insets 2 and 4

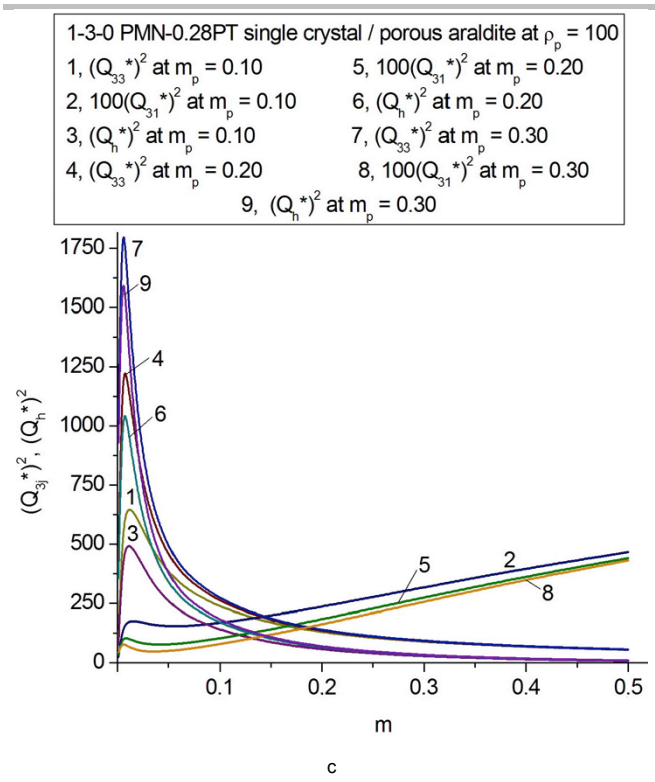

Figure 7 (continued)

in Fig. 1). The SC rods are in the form of a rectangular parallelepiped with a square base and square arrangement in the (X_1OX_2) plane, and the spontaneous polarisation of each rod is $\boldsymbol{P_s}^{(1)}$ || OX_3. The main crystallographic axes of each rod are oriented as follows: X || OX_1, Y || OX_2 and Z || OX_3. The shape of each ceramic inclusion (see C2c in the inset 4 in Fig. 1) obeys the equation

$$(x_1 / a_1)^2 + (x_2 / a_2)^2 + (x_3 / a_3)^2 = 1 \qquad (23)$$

in the axes of the co-ordinate system ($X_1X_2X_3$). In Eq. (23), a_1, $a_2 = a_1$ and a_3 are the semi-axes of each inclusion. Its aspect ratio is $\rho_i = a_1 / a_3$. We assume that the ceramic inclusions occupy sites of a simple tetragonal lattice with unit-cell vectors parallel to the OX_k axes. Assuming that the linear sizes of the inclusions in the 0–3 matrix are much smaller than the length of the side of the square rod cross section in the (X_1OX_2) plane (Fig. 1), we evaluate the effective properties of the 1–0–3 composite $\Pi^* = \Pi^*(m, m_i, \rho_i)$ in two stages.

In the first stage, we determine the effective properties of the 0–3 matrix by means of the effective field method, see Eq. (1). Hereby we take into account the interaction between the ceramic inclusions in the polymer matrix (see C2c and C2d in the inset 4 in Fig. 1). The || S || matrix from Eq. (1) contains the Eshelby tensor components [23] that depend on the elements of $||C^{(2)}||$ (polymer properties) and aspect ratio ρ_i of the ceramic inclusions. In the second stage, by analogy with the 1–3–0 composite, the effective properties of the studied 1–0–3 composite are evaluated in terms of the matrix method, using Eq. (4).

We now chose components with contrasting properties as follows. The PMN–0.33PT SC exhibits a very high piezoelectric activity and moderate piezoelectric anisotropy (see Table 1) and plays the role of the main FE component (C1, rods in the inset 2 in Fig. 1). The modified $PbTiO_3$ ceramic exhibits only a moderate piezoelectric activity, but has a large piezoelectric anisotropy, see Table 1. This ceramic component is used to form a system of aligned inclusions, see C2c in the inset 4 in Fig. 1. The 0–3 matrix contains modified $PbTiO_3$ ceramic inclusions in a polyurethane medium. Our evaluations of the properties of the 0–3 matrix suggest that it exhibits a low piezoelectric activity due to the presence of isolated FE ceramic inclusions at volume fractions $0 < m_i \leq 0.3$ and aspect ratios $0.01 \leq \rho_i \leq 100$. However even in a case of an ideal poling level of this matrix, the absolute values of its piezoelectric coefficients are relatively low whereby $|d_{3j}^{(m)}| < 10$ pC / N [16, 45], i.e., two orders-of-magnitude less than $|d_{3j}^{(1)}|$ of the PMN–0.33PT SC. Hereafter we neglect the piezoelectric activity of the 0–3 ceramic / polymer matrix in comparison to the piezoelectric activity of the SC rod and consider the ceramic inclusions in their unpoled state.

An example of the aspect-ratio (ρ_i) dependence of the squared figures of merit $(Q_{3j}^*)^2$ of the 1–0–3 composite is shown in Fig. 8. Despite the small volume fractions of the SC and ceramic components, we observe large changes in $(Q_{3j}^*)^2$ at

$$0.01 < \rho_i < 2. \qquad (24)$$

In the aspect-ratio range (24), the shape of the ceramic inclusions in the 0–3 matrix shown in the inset 4 in Fig. 1 changes from highly prolate ($\rho_i << 1$) to oblate ($\rho_i > 1$). Such changes in the microgeometry of the 0–3 matrix give rise to significant changes in its elastic properties [45] that have a strong influence on the piezoelectric properties and figures of merit of the 1–0–3 composite. An important correlation between the elastic compliance $s_{33}^{(m)}$ of the 0–3 matrix and the squared figure of merit $(Q_{33}^*)^2$ of the composite is observed [45], and this correlation stems from the important role of $s_{33}^{(m)}$ in the formation of the piezoelectric response of the 1–3-type composite along the poling axis. Moreover, the elastic anisotropy of the 0–3 matrix leads to a stronger link between $s_{33}^{(m)}$ and $(Q_{33}^*)^2$ [45]. In addition, as follows from results [45], the $s_{11}^{(m)} / s_{13}^{(m)}$ and $s_{11}^{(m)} / s_{33}^{(m)}$ ratios undergo major changes in the aspect-ratio range (25). In contrast to this, the $s_{11}^{(m)} / s_{12}^{(m)}$ ratio undergoes minor changes while the elastic compliances $s_{11}^{(m)}$ and $s_{12}^{(m)}$ are related to the elastic response of the 0–3 matrix along the OX_1 and OX_2 axes oriented perpendicular to the poling direction. This characteristic behaviour of the elastic compliances of the 0–3 matrix is a result of the active role of the ceramic component in forming the piezoelectric response of the 1–0–3 composite. As seen from Fig. 8, the influence of the ceramic component on the squared figures of merit $(Q_{3j}^*)^2$ takes place even at the volume fraction m_i = 0.05. We also state that the condition (17) holds for the studied 1–0–3 SC / ceramic / polymer composite.

3.4. Hydrostatic Parameters

The hydrostatic parameters from Eqs. (12)–(14) are to be taken into consideration in the context of the piezoelectric performance,

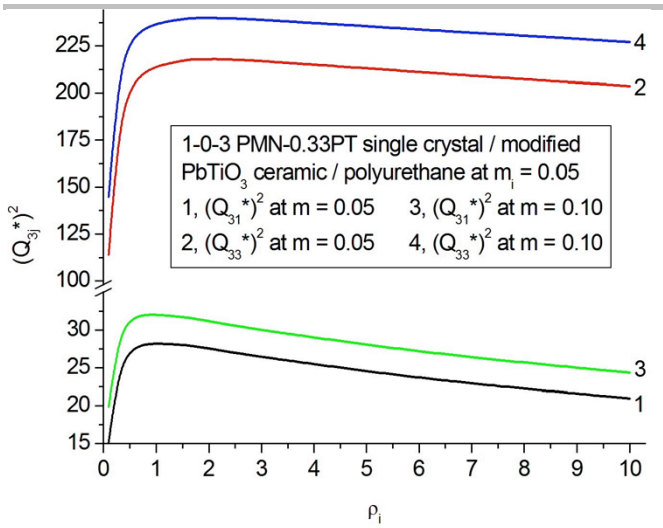

Figure 8. Effect of the aspect ratio of ceramic inclusions ρ_i on squared figures of merit $(Q_{3j}^*)^2$ (in 10^{-12} Pa^{-1}) of the 1–0–3 PMN–0.33 PT SC / modified $PbTiO_3$ ceramic / polyurethane composite

figures of merit and electromechanical coupling at a hydrostatic pressure. A specific conversion of the mechanical energy into electric energy is important in hydrophones and other hydroacoustic systems [2, 27]. Our results show that the large anisotropy of the piezoelectric coefficients d_{3j}^* and g_{3j}^* promotes large hydrostatic piezoelectric coefficients d_h^* and g_h^* from Eqs. (12) and related parameters from Eqs. (13) and (14) [3–5, 13, 45, 46, 48, 49], and this effect becomes pronounced in the presence of a heterogeneous matrix. In Section 3.4 we consider the hydrostatic piezoelectric performance of some 1–3-type composites wherein the heterogeneous matrix strongly influences the hydrostatic parameters.

In the first example, we consider the 1–0–3 composite [49, 50] that is characterised by the regular distribution of cylindrical ceramic rods (see the inset 1 in Fig. 1) and spheroidal ceramic inclusions in the polymer matrix (see the inset 4 in Fig. 1). The shape of each ceramic inclusion (see C2c in the inset 4 in Fig. 1) is described by Eq. (23). The composite as a whole is poled along the *OX*$_3$ axis. The determination of the effective properties of the composite is carried in two stages [13, 48]. First, the effective properties of the 0–3 matrix are evaluated as a function of ρ_i and m_i, and hereby the effective field method is applied, see Eq. (1). Second, the properties of the system "ceramic rods – heterogeneous matrix" are also evaluated as a function of m by means of the effective field method. By analogy with the 1–0–3 SC / ceramic / polymer composite described in Section 3.3, we neglect the piezoelectric activity of the 0–3 ceramic / polymer matrix [48] because its piezoelectric coefficients $|d_{3j}^{(m)}|$ remain much smaller than $|d_{3j}^{(1)}|$ of the poled ceramic rod.

Fig. 9 shows that a strong correlation between the hydrostatic piezoelectric coefficient d_h^* and ECF k_h^* is observed even in the presence of the same ceramic component in the rods and inclusions. Moreover, as follows from Table 1, the PCR-7M ceramic as a main FE component of this composite does not exhibit a large piezoelectric or elastic anisotropy. Eq. (14) suggests that the relation $k_h^* \sim d_h^*$ would hold irrespective of components and microgeometric features of a composite. Based

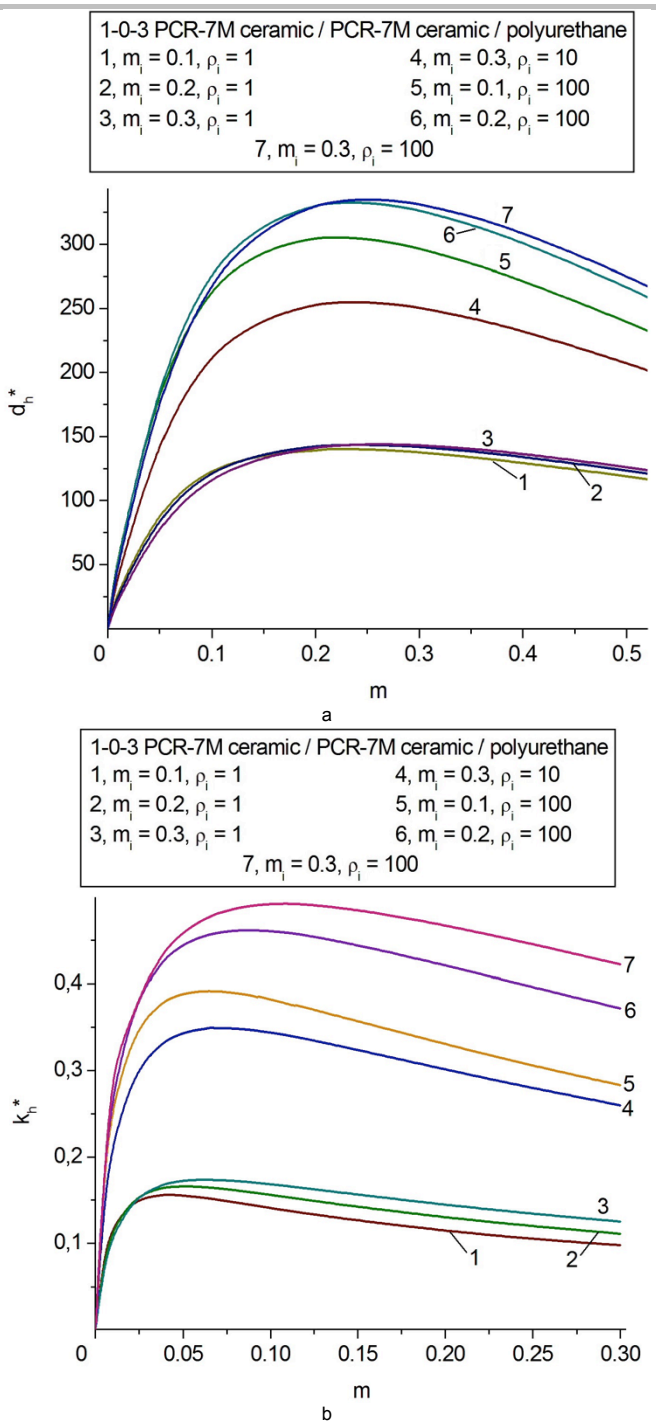

Figure 9. Correlation between the hydrostatic piezoelectric coefficient d_h^* (a, in pC / N) and hydrostatic ECF k_h^* (b) in the 1–0–3 PCR-7M ceramic / PCR-7M ceramic / polyurethane composite

on data in Fig. 9, we state that the larger d_h^* and k_h^* values are expected at a larger volume fraction m_i of heavily oblate ceramic inclusions ($\rho_i >> 1$); compare, for instance, curves 5–7 in Fig. 9, a and b. The system of heavily oblate inclusions in the 0–3 matrix leads to large elastic anisotropy, and the $s_{11}^{(m)}/s_{13}^{(m)}$ and $s_{11}^{(m)}/s_{33}^{(m)}$ ratios strongly influence the piezoelectric anisotropy of the 1–0–3 composite. Larger $(Q_h^*)^2$ values are also achieved at larger aspect ratio ρ_i. As follows from work [50], values of

max[$(Q_h^*)^2$] of the 1–0–3 composite based on PCR-7M are in the range (25–30)·10^{-12} Pa^{-1} at m_i = 0.1–0.3 and ρ_i = 100, and max[$(Q_h^*)^2$] is achieved at a ceramic rod volume fraction of $m \approx$ 0.05. We add that in accordance with data in Table 1, the poled PCR-7M ceramic is characterised by hydrostatic parameters d_h = 60 pC / N and $d_h g_h$ = 0.0827·10^{-12} Pa^{-1}. Undoubtedly, these values are much smaller than the related composite parameters near their maximum points; see curves 4–7 in Fig. 9, a.

We observe similar trends in the behaviour of $(Q_h^*)^2$ on consideration of the performance of the 1–3–0 composite based on the PMN–0.28PT SC (see curves 3, 6 and 9 in Fig. 7). The presence of prolate air pores in the polymer medium promotes smaller values of both $(Q_{33}^*)^2$ and $(Q_h^*)^2$ (Fig. 7, a) due to the less-favourable elastic anisotropy of the 3–0 matrix. In the presence of heavily oblate air pores in the 3–0 matrix, we achieve large $(Q_h^*)^2$ values, especially at m < 0.1 (Fig. 7, c).

The highly unusual example of the hydrostatic piezoelectric response of the 1–0–3 composite was studied in work [16]. This composite is similar to the 1–3–0 PMN–0.33PT SC / modified $PbTiO_3$ ceramic / polyurethane composite, however instead of the PMN–0.33PT SC, the PZN–0.08PT SC is used. As follows from Table 1, the PZN–0.08PT SC exhibits a high piezoelectric activity (e.g., the longitudinal piezoelectric coefficient d_{33} is the largest in the group of the relaxor-FE SCs), however the hydrostatic piezoelectric response is characterised by small negative values: d_h = –20 pC / N, g_h = –0.293 mV·m / N and k_h = –0.0258. Graphs in Fig. 10 show the important role of the 0–3 matrix in forming the hydrostatic response of the composite. Changes in the aspect ratio ρ_i, especially at ρ_i > 1, lead to considerable changes in d_h^* (Fig. 10, a) and k_h^* (Fig. 10, b), and the correlation between these hydrostatic parameters is obvious. Changes in sgn d_h^* (Fig. 10, a) and sgn k_h^* (Fig. 10, b) are observed at volume fractions of SC 0.9 < m < 1, when the SC rods play a dominating role in determining the piezoelectric properties of the composite. At ρ_i > 1, a lower dielectric permittivity of the 0–3 matrix $\varepsilon_{33}^{(m)}$ is achieved at m_i= const, and the inequality $\varepsilon_{33}^{(m)} << \varepsilon_{33}^{(1),\sigma}$ holds in wide m_i and ρ_i ranges. It should be noted that changes in the matrix elastic properties and their anisotropy become appreciable at ρ_i > 1 [16], and this favours a larger piezoelectric anisotropy and hydrostatic parameters (12)–(14) of the composite. Like d_h^*, the hydrostatic squared figure of merit $(Q_h^*)^2$ depends on the aspect ratio ρ_i to a large extent, and max[$(Q_h^*)^2$] at m_i = 0.1 takes the following values in 10^{-12} Pa^{-1}: 1.15 (at ρ = 0.01), 1.16 (at ρ = 0.1), (at ρ = 0.01), 6.71 (at ρ = 1), 25.3 (at ρ = 10), and 39.0 (at ρ = 100). This increase of the max[$(Q_h^*)^2$] values is in full agreement with the increase of max d_h^* in Fig. 10, a.

The effective parameters of the studied and related 1–3-type composites were compared to parameters evaluated by the finite element method [5, 13–15, 45, 51], and we do not consider results of comparison in detail. As follows from data [5, 13–15, 45, 51], agreement between the effective parameters calculated by different ways is achieved at various volume fractions of the FE component and inclusions, porosity levels and aspect ratios of inclusions.

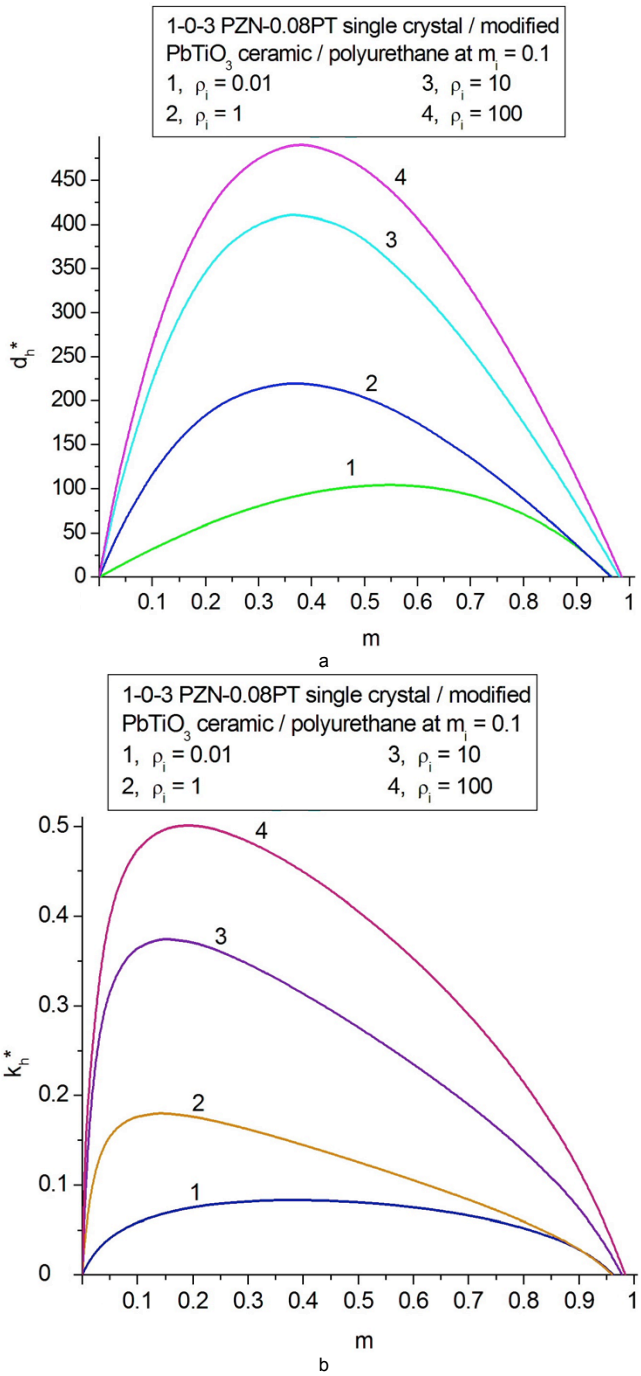

Figure 10. Correlation between the hydrostatic piezoelectric coefficient d_h^* (a, in pC / N) and hydrostatic ECF k_h^* (b) in the 1–0–3 PZN–0.08PT SC / modified $PbTiO_3$ ceramic / polyurethane composite

3.5. Manufacturing Methods for Piezoelectric Energy Harvesting

In the last decades, the techniques to manufacture piezo-active composites for energy-harvesting applications are also of interest to discuss. As follows from numerous literature data, there are four general methods for the widespread manufacture of 1–3-type piezo-active composites. Firstly, most commercial preparation methods are based on the ‘dice-and-fill’ technique

[52], where sawing through a ceramic or SC plate leads to the formation of thin parallel rods that become main piezoelectric components in the composites. This approach is suitable for the manufacture of both ceramic-based [20] and SC-based [53] composites. The rod sizes [54, 55], such as height and width, are typically ~10^{-5} m, and the rod shape [56, 57] can be rectangular, triangular or hexagonal and can be readily changed by a high resolution sawing machine and employing different cutting directions during the sawing process. One of the disadvantages of the process is that it can be time-consuming, with a possibility of cracking or damage of the slices and a large loss of ceramic material during the sawing and grinding processes (especially when the volume fraction *m* is small). The second approach to manufacture the 1–3-type composites is termed the 'laminate-and-cut' technique [58], where the piezo-active layer and piezo-passive layer are laminated separately and then cut twice to form the composite. Thirdly, another alternative, where there is no need for cutting, is the 'soft mould' method [59] where a reusable master mould that is structured by the microsystem technologies (such as advanced silicon etch process) would be used, followed by filling with the ceramic suspension, drying and sintering. This process is therefore most suitable for the ferroelectric polycrystalline ceramics rather than for the ferroelectric SCs. Finally, freeze casting is a relatively new route that has been effectively employed to achieve a 1–3-type composite architecture. The composite manufactured by this method consists of a system of piezo-active rods and air-based matrix prepared by using a solvent-based suspension [60, 61]. Due to this near-net forming process, there is no dicing or cutting procedure. The thickness and width of the piezo-active rod can be readily controlled by adjusting the freezing conditions and suspension rheological properties, providing the effective d_{33}^* values comparable to d_{33} of the monolithic component. These characteristics suggest that the manufactured composite can be applied in piezoelectric energy-harvesting devices.

Problems of the manufacturing of the 1–0–3 SC / ceramic / polymer composite were discussed in work [45]. Methods to form a 1–0–3 composite structure include the rod placement using a rod fixture [2, 62] and the independent preparation of the SC rods and heterogeneous 0–3 ceramic / polymer matrix with through-thickness holes for the long rods [63]. The independent preparation of ceramic rods and surrounding heterogeneous matrix has been employed for a 1–3–1 composite [63]. A formation of a porous structure in piezo-active composites and related materials [64–66] can lead to the large piezoelectric anisotropy and validity of condition (20). Hereby the piezoelectric performance of the porous materials based on conventional ferroelectric ceramics [e.g. Pb(Zr, Ti)O_3 in Ref. 64 or $BaTiO_3$ in Refs. 65 and 66] is described by taking into account 1–3–0 connectivity patterns.

3.6. Piezotechnical Energy-Harvesting Applications

In the present paper, we have considered the piezoelectric performance, electromechanical coupling and hydrostatic response of the piezo-active 1–3-type composites. Their parameters (Table 4) comprise the piezoelectric coefficients, ECFs, squared figures of merit, and anisotropy factors. These parameters indicate the significant potential of the studied 1–3-type in modern piezo-technical and energy-harvesting branches. The 1–3-type composites listed in Table 4 are based on either ferroelectric ceramics or domain-engineered SCs, and among the studied composites, one can single out the promising lead-free materials with 1–3 and 1–2–2 connectivities. It is believed that these and similar lead-free composites will be of interest in the field of piezoelectric energy harvesting due to sets of large effective parameters and due to electromechanical properties of SC components.

Table 4. Some effective parameters and applications of the studied 1–3-type composites

Composites	Effective parameters	Potential applications
1–3 PCR-7M / auxetic polyethylene	d_{33}^* and ζ_d*	Piezoelectric transducers, acoustic signal-echo antennae
	$(Q_{33}^*)^2$, condition (17)	Piezoelectric energy-harvesting devices
1–3 lead-free SC / auxetic polyethylene	g_{33}^*, condition (16)	Piezoelectric sensors, transducers and acoustic signal-echo antennae
	$(Q_{33}^*)^2$, condition (17)	Piezoelectric energy-harvesting devices
	g_h^* and $(Q_h^*)^2$	Hydrophones and hydroacoustic systems
1–3 PCR-7M / auxetic polyethylene	d_{33}^* and ζ_d*	Piezoelectric transducers, acoustic signal-echo antennae
1–3–0 PMN–0.33PT SC / porous polyurethane	d_{33}^* and ζ_d* at $\rho_p >> 1$	Piezoelectric actuators, transducers, and acoustic signal-echo antennae
1–2–2 KNNTL:Mn SC / polymer / polyethylene	d_{33}^*, condition (20)	Piezoelectric transducers
	g_{33}^*, condition (20)	Piezoelectric sensors
1–2–2 KNNTL:Mn SC / araldite / polyethylene	k_t^*, conditions (20) and (22)	Piezoelectric transducers
1–3–0 PMN–0.28 PT SC / porous araldite	$(Q_{33}^*)^2$, condition (17)	Piezoelectric energy-harvesting devices
	$(Q_h^*)^2$	Hydrophones and hydroacoustic systems
1–0–3 PMN–0.33 PT SC / modified $PbTiO_3$ ceramic / polyurethane	$(Q_{33}^*)^2$, condition (17)	Piezoelectric energy-harvesting devices
1–0–3 PCR-7M ceramic / PCR-7M ceramic / polyurethane	d_h^*, k_h^* and $(Q_h^*)^2$ at $\rho_l >> 1$	Hydrophones and hydroacoustic systems
1–0–3 PZN–0.08PT SC / modified $PbTiO_3$ ceramic / polyurethane	d_h^*, k_h^* and $(Q_h^*)^2$ at $\rho_l >> 1$	Hydrophones and hydroacoustic systems

4. Conclusions

The present paper has been devoted to modern piezo-active 1–3-type composites and their effective parameters that are important for piezoelectric transducer, hydroacoustic and

energy-harvesting applications. We have considered a number of examples of the piezoelectric anisotropy, electromechanical coupling factors (ECFs), squared figures of merit, and hydrostatic parameters in the composites based on either ferroelectric ceramics or single crystals. Among the composite systems of interest for piezoelectric energy-harvesting and related applications, we mention 1–3 SC / auxetic polymer, 1–2–2 SC / polymer / polymer, 1–0–3 SC / ceramic / polymer, and 1–3–0 SC / porous polymer. Examples of the connectivity patterns of technological interest are shown in Fig. 1. The composites listed in Table 4 and their parameters highlighted in the present paper (see, e.g. Figs. 2–10) enable us to underline their high performance and parameters that can be useful in energy-harvesting and related applications.

A remarkable observation is concerned with use of advanced lead-free components to form composites suitable for piezoelectric energy-harvesting, hydroacoustic and other applications. Important candidates among the high-performance 1–3-type composites are the KNN-TL SC / auxetic polyethylene, KNN-T SC / auxetic polyethylene and KNNTL:Mn SC / polymer-1 / polymer-2 composites. For certain parameters, these lead-free composites can be competitive compared to composites based on the domain-engineered relaxor-FE SCs, e.g. PMN–*x*PT or PZN–*x*PT which are listed in Table 1.

The important role of the microgeometry and elastic properties of the heterogeneous matrix (auxetic polymer and 3–0, 0–3 and 2–2 connectivity patterns) in determining the piezoelectric properties, ECFs and squared figures of merit of the 1–3-type composites has been emphasised, and the influence of the elastic anisotropy on the piezoelectric properties and anisotropy of these composites has been discussed.

In general, knowledge of the anisotropy factors (10), squared figures of merit (11), ECFs (6)–(9), and related parameters as well as their dependences on microgeometry and content of the composite are to be taken into account at the manufacturing of novel energy-harvesting materials with preferable directions for the conversion of energy and for the propagation of energy along specific directions.

Acknowledgements

The authors would like to thank Prof. Dr. A. E. Panich and Prof. Dr. A. A. Nesterov (Southern Federal University, Rostov-on-Don, Russia) for their continuing interest in the research problems. Prof. Dr. C. R. Bowen would like to acknowledge funding from the European Research Council under the European Union's Seventh Framework Programme (FP/2007-2013) / ERC Grant Agreement no. 320963 on Novel Energy Materials, Engineering Science and Integrated Systems (NEMESIS). In the present paper, the results on the research project No. 11.1627.2017/4.6 PCh have been represented within the framework of the state task in the scientific activity area at the Southern Federal University, and Prof. Dr. V. Yu. Topolov acknowledges funding with thanks. This research has been performed using the equipment of the Centre of Collective Use 'High Technologies' at the Southern Federal University. Dr. Y. Zhang would like to acknowledge the European Commission's Marie Skłodowska-Curie Actions (MSCA), through the Marie Skłodowska-Curie Individual Fellowships (IF-EF) (H2020-MSCA-IF-2015-EF-703950-HEAPPs) under Horizon 2020.

Keywords: composite • electromechanical properties • energy harvesting • piezoelectric anisotropy • effective parameters

[1] R. E. Newnham, *Mater. Res. Soc. Bull*. **1997**, *22* (5), 20-34.
[2] E. K. Akdogan, M. Allahverdi, A. Safari, *IEEE Trans. Ultrason. Ferroelectr. Freq. Control* **2005**, *52*, 746-775.
[3] V. Yu. Topolov, C. R. Bowen, *Electromechanical Properties in Composites Based on Ferroelectrics*, Springer, London, **2009**.
[4] C. R. Bowen, V. Yu. Topolov, H. A. Kim, *Modern Piezoelectric Energy-Harvesting Materials*, Springer International Publishing Switzerland, **2016**.
[5] C. R. Bowen, V. Yu. Topolov, A. N. Isaeva, P. Bisegna, *CrystEngComm* **2016**, *18*, 5986-6001.
[6] R. Zhang, B. Jiang, W. Cao, *J. Appl. Phys*. **2001**, *90*, 3471-3475.
[7] X. Huo, R. Zhang, L. Zheng, S. Zhang, R. Wang, J. Wang, S. Sang, B. Yang, W. Cao, *J. Am. Ceram. Soc*. **2015**, *98*, 1829-1835.
[8] T. Ikeda, *Fundamentals of Piezoelectricity*, Oxford University Press, Oxford, New York, Toronto, **1990**.
[9] K. Ren, Y. Liu, X. Geng, H. F. Hofmann, Q. M. Zhang, *IEEE Trans. Ultrason. Ferroelectr. Freq. Control* **2008**, *53*, 631-638.
[10] F. Wang, C. He, Y. Tang, X. Zhao, H. Luo, *Mater. Chem. Phys*. **2007**, *105*, 273-277.
[11] R. E. Newnham, D. P. Skinner, L. E. Cross, *Mater. Res. Bull*. **1978**, *13*, 525-536.
[12] V. Yu. Topolov, S. V. Glushanin, *J. Phys. D: Appl. Phys*. **2002**, *35*, 2008-2014.
[13] V. Yu. Topolov, P. Bisegna, C. R. Bowen, *Piezo-Active Composites. Orientation Effects and Anisotropy Factors*, Springer, Berlin, Heidelberg, **2014**.
[14] V. Yu. Topolov, A. V. Krivoruchko, P. Bisegna, *Composites Sci. Technol*. **2011**, *71*, 1082-1088.
[15] V. Yu. Topolov, C. R. Bowen, P. Bisegna, A. V. Krivoruchko, *Mater. Chem. Phys*. **2015**, *151*, 187-195.
[16] V. Yu. Topolov, C. R. Bowen, P. Bisegna, A. E. Panich, *Funct. Mater. Lett*. **2015**, *8*, 1550049.
[17] V. Yu. Topolov, S. E. Filippov, P. Bisegna, *Ferroelectrics* **2012**, *432*, 92-102.
[18] S-H. Zhai, Y.-C. Wang, B. Geng, H.-C. Xu, S.-F. Huang in *2016 Symposium on Piezoelectricity, Acoustic waves, and Device Applications, Oct. 21-24, Xi'an, Shaanxi, China*, IEEE, **2015**, pp. 37-40.
[19] S. Huang, M. Sun, M. Zhou, D. Xu, Q. Li, X. Cheng, *Mater. Manufact. Processes* **2015**, *30*, 179-183.
[20] R. Rouffaud, F. Levassort, M. P. Thi, C. Bantignies, M. Lethiecq, A.-C. Hladky-Hennion, *IEEE Trans. Ultrason. Ferroelectr. Freq. Control* **2016**, *63*, 2215-2223.
[21] V. Yu. Topolov, P. Bisegna, *J. Electroceram*. **2010**, *25*, 26-37.
[22] V. Yu. Topolov, A. V. Krivoruchko, P. Bisegna, C. R. Bowen, *Ferroelectrics* **2008**, *376*, 140-152.
[23] J. H. Huang, S. Yu, *Composites Engin*. **1994**, *4*, 1169-1182.
[24] F. Levassort, M. Lethiecq, C. Millar, L. Pourcelot, *IEEE Trans. Ultrason. Ferroelectr. Freq. Control* **1998**, *45*, 1497-1505.
[25] F. Levassort, V. Yu. Topolov, M. Lethiecq, *J. Phys. D: Appl. Phys*. **2000**, *33*, 2064-2068.
[26] L. V. Gibiansky, S. Torquato, *J. Mech. Phys. Solids* **1997**, *45*, 689-708.
[27] C. H. Sherman, J. L. Butler, *Transducers and Arrays for Underwater Sound*, Springer, New York, **2007**.
[28] H. Kim, Y. Tadesse, S. Priya in *Energy Harvesting Technologies* (Eds.: S. Priya, D. J. Inman), Springer, New York, **2009**, pp 3-39.
[29] K. Uchino, T. Ishii, *Ferroelectrics* **2010**, *400*, 305-320.
[30] S. Priya, *IEEE Trans. Ultrason. Ferroelectr. Freq. Control* **2010**, *57*, 2610-2612.
[31] R. Zhang, W. Jiang, B. Jiang, W. Cao in *Fundamental Physics of Ferroelectrics* (Ed.: R. E. Cohen), American Institute of Physics, Melville, **2002**, pp. 188-197.
[32] S. Zhang, J. Luo, W. Hackenberger, T. R. Shrout, *J. Appl. Phys*. **2006**, *104*, 064106.
[33] G. Liu, W. Jiang, J. Zhu, W. Cao, *Appl. Phys. Lett*. **2011**, *99*, 162901.

[34] J. Yin, B. Jiang, W. Cao, *IEEE Trans. Ultrason. Ferroelectr. Freq. Control* **2000**, *47*, 285-291.

[35] R. Zhang, B. Jiang, W. Cao, A. Amin, *J. Mater. Sci. Lett*. **2002**, *21*, 1877-1879.

[36] L. M. Zheng, X. Q. Huo, R. Wang, J. J. Wang, W. H. Jiang, W. W. Cao, *CrystEngComm* **2013**, *15*, 7718-7722.

[37] X. Huo, L. Zheng, R. Zhang, R. Wang, J. Wang, S. Sang, Y. Wang, B. Yang, W. Cao, *CrystEngComm* **2014**, *16*, 9828-9833.

[38] J. H. Huang, W.-S. Kuo, *Acta Mater*. **1996**, *44*, 4889-4898.

[39] S. Ikegami, I. Ueda, T. Nagata, *J. Acoust. Soc. Am*. **1971**, *50*, 1060-1066.

[40] A. A. Grekov, S. O. Kramarov, A. A. Kuprienko, *Mech. Compos. Mater*. **1989**, *25*, 54-61.

[41] K. E. Evans, K. L. Alderson, *J. Mater. Sci. Lett*. **1992**, *11*, 1721-1724.

[42] I. N. Groznov in *Physics Encyclopaedia*, Sovetskaya Entsiklopediya, Moscow, **1983**, pp. 178-179 (in Russian).

[43] V. Yu. Topolov, C.R. Bowen, *Mater. Lett*. **2015**, *142*, 265-268.

[44] M. L. Dunn, M. Taya, *J. Am. Ceram. Soc*. **1993**, *76*, 1697-1706.

[45] V. Yu. Topolov, C. R. Bowen, P. Bisegna, *Sens. Act. A* **2015**, *229*, 94-103.

[46] V. Yu. Topolov, A. V. Turik, *Tech. Phys*. **2001**, *46*, 1093-1100.

[47] S. H. Choy, H. L. W. Chan, M. W. Ng, P. C. K. Liu, *Integr. Ferroelectrics* **2004**. *63*, 109-115.

[48] V. Yu. Topolov, C. R. Bowen, S. E. Filippov, *Ferroelectrics* **2012**, *430*, 92-97.

[49] V. Yu. Topolov, C. R. Bowen, S. E. Filippov, A. A. Vorontsov, *Integr. Ferroelectrics* **2012**, *133*, 91-95.

[50] V. Yu. Topolov, S. E. Filippov, A. A. Vorontsov, *Nano- i Mikrosistemnaya Tekhnika* **2011**, No. 9, 13-19 (in Russian).

[51] V. Yu. Topolov, C. R. Bowen, P. Bisegna in *Advanced Materials. Manufacturing, Physics, Mechanics and Applications* (Eds.: I. A. Parinov, S.-H. Chang, V. Yu. Topolov), Springer, Cham, Heidelberg, New York, Dordrecht, London, **2016**, pp.179-195.

[52] H. P. Savakus, K. A. Klicker, R. E. Newnham. *Mater. Res. Bull.* **1981**, *16*, 677-680.

[53] D. Zhou, K. F. Cheung, Y. Chen, S. T. Lau, Q. Zhou, K. Shung, H. S. Luo, J. Dai, H. L. W. Chan, *IEEE Trans. Ultrason. Ferroelectr. Freq. Control* **2011**, *58*, 477-484.

[54] R. Xie, Y. Zhao, K. C. Zhou, D. Zhang, Y. Wang, H. L. W. Chan. *J. Amer. Cer. Soc*. **2014**, *97*, 2590-2595.

[55] Y. Xu, J. F. Li, J. Ma, C. W. Nan, *J. Phys. D: Appl. Phys*. **2012**, *45*, 315306.

[56] J. Yin, M. Lee, J. Brown, E. Chérin, F. Foster. *IEEE Trans. Ultrason. Ferroelectr. Freq. Control* **2010,** *57*, 957-968.

[57] J. Dziewierz, S. N. Ramadas, A. Gachagan, R. L. O'Leary, G. Hayward, *IEEE Ultrasonics Symp*. **2009**, 422-425.

[58] W. A. Smith, Proc. *IEEE Ultrasonics Symp*. **1989**, 755-766.

[59] S. Starke, A. Schönecker, W. Gebhardt. *IEEE Ultrasonics Symp*. **2016,** 1-4.

[60] R. Guo, C. A. Wang, A. K. Yang, J. T. Fu, *J. Appl. Phys.* **2010**, *108*, 124112.

[61] R. Guo, C. A. Wang, A. K. Yang, *J. Am. Ceram. Soc.* **2011**, *94*, 1794-1799.

[62] K.A. Klicker, J.V. Biggers, R.E. Newnham, *J. Am. Ceram. Soc*. **1981**, *64*, 5–9.

[63] C. Richard, *Étude expérimentale et théorique de composites piézoélectriques de connectivité 1.3.1 pour hydrophone*, Institut National des Sciences Appliquées de Lyon, Lyon, **1992** (Thesis).

[64] S. E. Filippov, A. A. Vorontsov, O. E. Brill, V. Yu. Topolov, *Funct. Mater. Lett.* **2014**, *7*, 1450029.

[65] J. I. Roscow, V. Yu. Topolov, C. R. Bowen, J. Taylor, A. E. Panich, *Sci. a. Technol. Adv. Mater.* **2016**, *17*, 769-776.

[66] J. I. Roscow, V. Yu. Topolov, J. T. Taylor, C. R. Bowen. *Smart Mater. Struct.* **2017** (in press).